

---

# STATE, GLOBAL AND LOCAL PARAMETER ESTIMATION USING LOCAL ENSEMBLE KALMAN FILTERS: APPLICATIONS TO ONLINE MACHINE LEARNING OF CHAOTIC DYNAMICS

---

PREPRINT

**Quentin Malartic**

CEREA, École des Ponts and EDF R&D  
Île-de-France, France  
and

LMD/IPSL, ENS, PSL Université, École Polytechnique,  
Institut Polytechnique de Paris, Sorbonne Université, CNRS,  
Paris, France  
quentin.malartic@enpc.fr

**Alban Farchi**

CEREA, École des Ponts and EDF R&D  
Île-de-France, France  
alban.farchi@enpc.fr

**Marc Bocquet**

CEREA, École des Ponts and EDF R&D  
Île-de-France, France  
marc.bocquet@enpc.fr

July 27, 2021

**ABSTRACT**

In a recent methodological paper, we have shown how to learn chaotic dynamics along with the state trajectory from sequentially acquired observations, using local ensemble Kalman filters. Here, we more systematically investigate the possibility to use a local ensemble Kalman filter with either covariance localization or local domains, in order to retrieve the state and a mix of key global and local parameters. Global parameters are meant to represent the surrogate dynamics, for instance through a neural network, which is reminiscent of data-driven machine learning of dynamics, while the local parameters typically stand for the forcings of the model. A family of algorithms for covariance and local domain localization is proposed in this joint state and parameter filter context. In particular, we show how to rigorously update global parameters using a local domain EnKF such as the LETKF, an inherently local method. The approach is tested with success on the 40-variable Lorenz model using several of the local EnKF flavors. A two-dimensional illustration based on a multi-layer Lorenz model is finally provided. It uses radiance-like non-local observations, and both local domains and covariance localization in order to learn the chaotic dynamics, the local forcings, and the couplings between layers. This paper more generally addresses the key question of online estimation of both global and local model parameters.

**Keywords** local ensemble Kalman filters · LEnSRF · LETKF · parameter estimation · machine learning · data-driven dynamics · chaotic dynamics

# 1 Introduction

## 1.1 Parameter estimation and data-driven techniques for the geosciences

The recent upheaval generated by machine learning (ML) and in particular deep learning has opened the way to a wealth of data-driven techniques, where not only the state of an observed dynamical system is estimated but also its key dynamical constitutive parameters, if not the full model. There are by mid 2021, dozens of ML papers in the literature dealing with the problem of estimating the dynamics of a system from observation, even when only focusing on typical low-order models used in the field of geoscience. The problem can be addressed by typical ML techniques, such as the projection on a regressor frame or basis, random forests, analogs, diffusion maps, echo state networks, LSTM and other neural network approaches (Brunton *et al.*, 2016; Lguensat *et al.*, 2017; Harlim, 2018; Pathak *et al.*, 2018; Dueben and Bauer, 2018; Fablet *et al.*, 2018; Scher and Messori, 2019; Weyn *et al.*, 2019; Arcomano *et al.*, 2020). It can also be solved using a conjunction of ML and data assimilation (DA) techniques to exploit noisy and incomplete observations such as those met in realistic geoscience systems (Bocquet *et al.*, 2019; Brajard *et al.*, 2020; Bocquet *et al.*, 2020a; Arcucci *et al.*, 2021). In the case of high-dimensional systems, the relative lack of information can be compensated by additionally using past trajectories or information on the system such as an approximate model derived from physical laws (Wikner *et al.*, 2020; Brajard *et al.*, 2021; Farchi *et al.*, 2021b).

However, this should not divert us from the even much more abundant contributions focused on the problem of parameter estimation in meteorology and climate, oceanography, atmospheric chemistry, glaciology, hydrology, solid earth physics, space weather, seismology, etc., using more traditional DA and inverse problem techniques. Compared to the ML view, this part of the geoscience and applied mathematics literature relies much more on a trusted numerical physical model of the system under scrutiny in order to make inferences.

The merits of the ML scientific tsunami are to have blurred the frontiers between ML and DA approaches. Model error estimation, a classical topic of DA, where the main model is to be corrected through statistical procedures or via parameter estimation techniques, can now be addressed by the addition of an ML based correction with many parameters that need to be learned. Hence, the coming of ML has pushed the limits of what was traditionally asked of DA.

This paper is targeted at that ML/DA frontier where a part or the whole model needs to be learned. In addition, following (Bocquet *et al.*, 2020b), we aim at the difficult objective of learning state and parameters on the fly, *i.e.* online as observations are acquired, using sequential DA techniques such as the ensemble Kalman filter (EnKF) (Evensen, 2009), setting aside the variational methods which are much more common for parameter and ML problems (Farchi *et al.*, 2021a).

## 1.2 Local and global model parameters

In this paper, we assume that the parameters are not directly observed, which is a common but implicit assumption in the geosciences. Their inference necessarily indirectly stems from the observation of the state variables.

In an ensemble-based parameter estimation problem, a popular and universal trick consists in augmenting the state vectors to incorporate the parameters (Jazwinski, 1970). We have adopted it in (Bocquet *et al.*, 2020b) and we will keep doing so here. It was shown that this method also seamlessly blends well with ensemble-variational DA approaches (Bocquet and Sakov, 2013; Bocquet *et al.*, 2020b). One can distinguish between two types of parameters, whose nature have a significant impact on the EnKF-based approaches.

First, one can consider the *global* parameters, that do not depend on space. They can be parameters of the intrinsic physics of the geophysics fluid or of its dynamics. However, they are very different from the intrinsically local state variable, leading to substantial theoretical complications, especially when local EnKFs (LEnKFs) based on domain localization such as the local ensemble transform Kalman filter (LETKF) are used. This point has been addressed in (Bocquet *et al.*, 2020b) to a large extent, although additional numerical tests and theoretical improvement will be proposed here.

Second, *local* parameters are in a sense simpler to estimate as they are of the same nature as the state variables. However, their number can increase dramatically depending on the number of domains, and yield significantly larger augmented control vectors. The topic was not addressed in (Bocquet *et al.*, 2020b) but in earlier contributions to the literature (see below).

In this paper, we will consider both global and local parameters and develop new EnKF-based algorithms, accounting for the need of localization in high-dimensional systems. We will also consider simultaneously both type of parameters. Local parameters typically represent forcings (radiative forcing, species emissions, etc.) or a Coriolis term while global parameters would represent the parameterized dynamics and micro-physics.

Table 1: Adequacy and inadequacy between LEnKF types and the estimation of local and global parameter.

LEnKF type	Global parameters	Local parameters	Mixed set of parameters
LEnSRF (CL)	well suited localization in parameter space?	suited numerically costly	unclear solution proposed here
LETKF (DL)	only approximate solution proposed here	well suited	unclear solution proposed here

Moreover, in this paper, the parameters are assumed not to depend on time. This could be induced by an autonomous system, or it could be due to a known and explicit, parameterized dependence on time of, *e.g.*, the forcings, which would be themselves tuned by static parameters.

### 1.3 Parameter estimation techniques in the data assimilation geoscience literature

Although the literature on parameter estimation based on the EnKF applied to geosciences in high dimensions is vast, the set of available techniques is rather limited. To our knowledge, the state augmentation principle is always used. Ruiz, Pulido and Miyoshi have written a pedagogical review on parameter estimation with the EnKF (Ruiz *et al.*, 2013), which explains the mechanisms at play. Significant issues with the algorithms arise when local EnKFs are considered. In principle, LEnKFs with covariance localization (CL) handle global parameters well. However, the extension of the localization operator to the global parameters is not natural, while the addition of local parameters could have an excessive numerical cost. By contrast, LEnKFs with domain localization (DL) handle local parameters very well but fail at rigorously estimating global parameters.

The latter issue, of considerable importance, has been approximately addressed. In (Aksoy *et al.*, 2006; Fertig *et al.*, 2009; Hu *et al.*, 2010), the global parameters are made local in the DL update step and their local approximations are later averaged in space to form new global parameters (an ad hoc procedure) in order to propagate the ensemble using these updated global parameters.

The former issue where global parameters are estimated with CL LEnKFs, and which requires a definition of the localization matrix in parameter space as well as the cross-correlations, has been studied in (Koyama and Watanabe, 2010; Ruckstuhl and Janjić, 2018). The authors actually proposed a uniform localization whenever global parameters are concerned. The correlation and cross-correlation of the localization matrix could be set to 1 (absence of localization for the global parameters) or to a specific tapering scalar coefficient, which would additionally ensure the positive definiteness of the localization matrix (Ruckstuhl and Janjić, 2018).

In (Bocquet *et al.*, 2020b), following these first papers, several solutions have been proposed and tested for the CL LEnKF family. Moreover, theoretical solutions were proposed for the DL LEnKF family beyond the approximate solution of (Aksoy *et al.*, 2006), but with no numerical tests. These new types of EnKF were termed EnKFs-ML since they were meant to estimate not only the state but also the dynamics (through their parameters). Table 1 summarizes the adequacy and inadequacy between EnKF families and local/global parameters.

Here we will more systematically investigate the CL and DL LEnKFs-ML with global and local parameters. Filling in the gaps of the DA literature, we will propose new algorithms or algorithms that improve on the previous ones.

### 1.4 Outline of the paper

The paper is organized as follows. Our new algorithms are introduced and justified in section 2, experimental results are discussed in section 3 on a one-dimensional chaotic model and in section 4 on a two-dimensional chaotic model with non-local observations, and the conclusions follow in section 5.

## 2 Algorithms

Following (Bocquet *et al.*, 2020b), the algorithms derived and used in this article are based on the augmented EnKF. The main idea is to extend the state vector  $\mathbf{x} \in \mathbb{R}^{N_x}$  to  $\mathbf{z} \in \mathbb{R}^{N_z}$  containing the state variables and all model parameters. The strength of this approach is that correlations between state variables and parameters will develop during the assimilation cycles. Hence the parameters get corrected during the analysis steps even though they are not observed. During the forecast steps, the state variables are updated using the parameterized model, while the parameters follow persistence, *i.e.* are not updated.

Without localization, the implementation of the ML-counterpart of an EnKF algorithm, the EnKF-ML, is very similar to that of this original algorithm, provided that the observation operator  $\mathbf{H}$  has been adjusted for  $\mathbf{z}$  instead of  $\mathbf{x}$ . Hence,

in order to avoid divergence, the ensemble size must be strictly larger than the number of neutral and unstable modes of the total (state and parameter) dynamics, equal to the number of neutral and unstable modes of the state dynamics plus the number of influential and independent parameters, as explained in (Bocquet *et al.*, 2020b). Indeed, the parameter dynamics is entirely neutral since parameters are not updated during the forecast steps (Bocquet *et al.*, 2020b).

However adding localization to an EnKF-ML algorithm is not obvious because global parameters cannot in theory be localized. Exploiting the fact that parameters are not observed, we have shown that the EnKF-ML analysis can be written as a two-step process (Bocquet *et al.*, 2020b): (i) update the state using the observations and (ii) compute the parameter update from the state update using a linear regression based on the ensemble.

More generally, the posterior probability density function (pdf)  $p(\mathbf{z}|\mathbf{y})$ , which synthetizes the analysis problem, can be written

$$p(\mathbf{z}|\mathbf{y}) = p(\mathbf{x}, \mathbf{p}|\mathbf{y}) = p(\mathbf{p}|\mathbf{x}, \mathbf{y}) p(\mathbf{x}|\mathbf{y}) = p(\mathbf{p}|\mathbf{x}) p(\mathbf{x}|\mathbf{y}), \quad (1)$$

where it has been assumed that the parameter vector  $\mathbf{p}$  is independent of the observation vector  $\mathbf{y}$  conditional on  $\mathbf{x}$ . Hence, the analysis can be first carried out on  $\mathbf{x}$  by considering the marginal problem on  $\mathbf{x}$ , integrating out eq. (1) over  $\mathbf{p}$ , and later solving the problem on  $\mathbf{p}$  once it is solved on  $\mathbf{x}$ . A consequence of this decomposition is that localization can be enabled as usual for the state update and disabled for the parameter update. Nevertheless, such an update scheme may be sub-optimal if some of the parameters can be localized.

In the following sections, we extend the local EnKF-ML algorithms introduced in (Bocquet *et al.*, 2020b) and apply localization to the parameter update when possible. The resulting algorithms are called EnKF-HML (for *hybrid* ML) to emphasize the fact that the ML part is partly localized and partly non-localized. Both CL and DL are presented using the example of the ensemble square root Kalman filter (EnSRF) in the first case and of the ensemble transform Kalman filter (ETKF) in the second case (Evensen, 2009).

## 2.1 Methods and algorithms

### 2.1.1 Partitioning of the augmented space

We assume that the augmented state  $\mathbf{z} \in \mathbb{R}^{N_z}$  is organized as follows:

$$\mathbf{z} \triangleq \begin{bmatrix} \mathbf{x} \\ \mathbf{p} \\ \mathbf{q} \end{bmatrix}, \quad (2)$$

where  $\mathbf{x} \in \mathbb{R}^{N_x}$  is the state of the dynamical system,  $\mathbf{p} \in \mathbb{R}^{N_p}$  is the vector of *global* model parameters, and  $\mathbf{q} \in \mathbb{R}^{N_q}$  is the vector of *local* model parameters. The ensemble of the filter is a collection of  $N_e$  augmented states  $\{\mathbf{z}_i, i = 1, \dots, N_e\}$ . It is organized column-wise into the augmented ensemble matrix  $\mathbf{E} \in \mathbb{R}^{N_z \times N_e}$ . The augmented state mean  $\bar{\mathbf{z}} \in \mathbb{R}^{N_z}$  and the augmented state perturbation matrix  $\mathbf{X} \in \mathbb{R}^{N_z \times N_e}$  are defined by

$$\bar{\mathbf{z}} \triangleq \mathbf{E}\mathbf{1}/N_e, \quad (3a)$$

$$\mathbf{X} \triangleq (\mathbf{E} - \bar{\mathbf{z}}\mathbf{1}^\top) / \sqrt{N_e - 1}, \quad (3b)$$

where  $\mathbf{1} \in \mathbb{R}^{N_e}$  is the vector full of ones.

Following eq. (2),  $\mathbf{E}$ ,  $\bar{\mathbf{z}}$  and  $\mathbf{X}$  can be split according to the state ( $\mathbf{x}$ ), global parameter ( $\mathbf{p}$ ), and local parameter ( $\mathbf{q}$ ) subspaces into

$$\mathbf{E} = \begin{bmatrix} \mathbf{E}_x \\ \mathbf{E}_p \\ \mathbf{E}_q \end{bmatrix}, \quad \bar{\mathbf{z}} = \begin{bmatrix} \bar{\mathbf{x}} \\ \bar{\mathbf{p}} \\ \bar{\mathbf{q}} \end{bmatrix}, \quad \text{and} \quad \mathbf{X} = \begin{bmatrix} \mathbf{X}_x \\ \mathbf{X}_p \\ \mathbf{X}_q \end{bmatrix}. \quad (4)$$

For these quantities, an  $f$  superscript is used to refer to the forecast (or prior) value and an  $a$  superscript is used to refer to the analysis (or posterior) value. Using the same rationale, any matrix  $\mathbf{A} \in \mathbb{R}^{N_z \times N_z}$  can also be split into

$$\mathbf{A} = \begin{bmatrix} \mathbf{A}_{xx} & \mathbf{A}_{xp} & \mathbf{A}_{xq} \\ \mathbf{A}_{px} & \mathbf{A}_{pp} & \mathbf{A}_{pq} \\ \mathbf{A}_{qx} & \mathbf{A}_{qp} & \mathbf{A}_{qq} \end{bmatrix}. \quad (5)$$

In particular, this is the case of the prior error covariance matrix  $\mathbf{B}$  and of the localization matrix  $\rho$  for the EnSRF algorithm.

Furthermore, since the model parameters are not observed, the (potentially nonlinear) augmented observation operator  $\mathbf{H}$  can be written as

$$\mathbf{H} = \begin{bmatrix} \mathbf{H}_x \\ \mathbf{0} \\ \mathbf{0} \end{bmatrix}, \quad (6)$$

where  $\mathbf{H}_x$  is the *usual* observation operator, in such a way that the observation equation becomes

$$\mathbf{y} = \mathbf{H}(\mathbf{z}) = \mathbf{H}_x(\mathbf{x}). \quad (7)$$

Finally note that, in the following sections, the *matrices*  $\mathbf{H}_x$  and  $\mathbf{H}$  refer to the tangent linear of the maps  $\mathbf{x} \mapsto \mathbf{H}_x(\mathbf{x})$  and  $\mathbf{z} \mapsto \mathbf{H}(\mathbf{z})$ .

### 2.1.2 Matrix square root

Both the EnSRF and the ETKF are deterministic implementations of the EnKF which rely on a matrix square root. Several definitions of the matrix square root are possible, some of them being non equivalent. In this paper, we use the following definition, chosen *e.g.* in (Bocquet and Farchi, 2019; Farchi and Bocquet, 2019).

Let  $\mathbf{A}$  be a diagonalizable matrix with non-negative eigenvalues, written  $\mathbf{A} = \mathbf{G}\mathbf{D}\mathbf{G}^{-1}$ , where  $\mathbf{G}$  is an invertible matrix and  $\mathbf{D}$  a diagonal matrix with non-negative elements (the eigenvalues of  $\mathbf{A}$ ). The square root of  $\mathbf{A}$ , written  $\mathbf{A}^{1/2}$ , is defined as

$$\mathbf{A}^{1/2} \triangleq \mathbf{G}\mathbf{D}^{1/2}\mathbf{G}^{-1}, \quad (8)$$

where  $\mathbf{D}^{1/2}$  is the diagonal matrix containing the square root of the entries of  $\mathbf{D}$ , *i.e.* the square root of the eigenvalues of  $\mathbf{A}$ .

## 2.2 The ensemble square root Kalman filter

### 2.2.1 Generic (local) EnSRF analysis

The generic<sup>1</sup> EnSRF analysis is given by the following set of equations:

$$\bar{\mathbf{z}}^a = \bar{\mathbf{z}}^f + \mathbf{B}\mathbf{H}^\top \left( \mathbf{R} + \mathbf{H}\mathbf{B}\mathbf{H}^\top \right)^{-1} (\mathbf{y} - \mathbf{H}(\bar{\mathbf{z}}^f)), \quad (9a)$$

$$\mathbf{X}^a = \left( \mathbf{I} + \mathbf{B}\mathbf{H}^\top \mathbf{R}^{-1} \mathbf{H} \right)^{-1/2} \mathbf{X}^f. \quad (9b)$$

Equation (9a) is known as the *mean update* and eq. (9b) as the *perturbation update*. In these equations,  $\mathbf{B} \in \mathbb{R}^{N_z \times N_z}$  is the prior error covariance matrix, equal in this case to the forecast sample covariance matrix:

$$\mathbf{B} \triangleq \mathbf{X}^f (\mathbf{X}^f)^\top. \quad (10)$$

Although  $\mathbf{I} + \mathbf{B}\mathbf{H}^\top \mathbf{R}^{-1} \mathbf{H}$  may not be symmetric, it is diagonalizable with non-negative eigenvalues (see for instance (Farchi and Bocquet, 2019)), which makes the matrix square root in eq. (9b) well defined.

Following (Bocquet and Farchi, 2019), it can be shown using the matrix shift lemma (see for instance (Asch *et al.*, 2016), section 6.4.4) that the perturbation update eq. (9b) is equivalent to

$$\mathbf{X}^a = \mathbf{X}^f - \mathbf{B}\mathbf{H}^\top \left\{ \mathbf{R} + \mathbf{H}\mathbf{B}\mathbf{H}^\top + \mathbf{R} \left( \mathbf{I} + \mathbf{R}^{-1} \mathbf{H}\mathbf{B}\mathbf{H}^\top \right)^{1/2} \right\}^{-1} \mathbf{H}(\mathbf{X}^f), \quad (11)$$

where the linear algebra (matrix square root and inverse) is expressed in the observation space, which is usually much smaller than the augmented state space ( $N_y \ll N_z$ ), and where the secant method is used to compute  $\mathbf{H}(\mathbf{X}^f)$ . Furthermore, the EnSRF analysis eq. (9) can be written using the following incremental formulation in observation space:

$$\Delta \bar{\mathbf{z}} \triangleq \bar{\mathbf{z}}^a - \bar{\mathbf{z}}^f = \mathbf{B}\mathbf{H}^\top \left( \mathbf{R} + \mathbf{H}\mathbf{B}\mathbf{H}^\top \right)^{-1} (\mathbf{y} - \mathbf{H}(\bar{\mathbf{z}}^f)), \quad (12a)$$

$$\Delta \mathbf{X} \triangleq \mathbf{X}^a - \mathbf{X}^f = -\mathbf{B}\mathbf{H}^\top \left\{ \mathbf{R} + \mathbf{H}\mathbf{B}\mathbf{H}^\top + \mathbf{R} \left( \mathbf{I} + \mathbf{R}^{-1} \mathbf{H}\mathbf{B}\mathbf{H}^\top \right)^{1/2} \right\}^{-1} \mathbf{H}(\mathbf{X}^f). \quad (12b)$$

This update can be further simplified if  $\mathbf{R}^{-1/2}$  is easy to compute, for instance if  $\mathbf{R}$  is diagonal as is often assumed in the geosciences. In this case, let us introduce the ancillary matrix  $\mathbf{T} \in \mathbb{R}^{N_y \times N_y}$  defined as

$$\mathbf{T} \triangleq \mathbf{I} + \mathbf{R}^{-1/2} \mathbf{H}\mathbf{B}\mathbf{H}^\top \mathbf{R}^{-1/2}. \quad (13)$$

<sup>1</sup>The term *generic* is used to describe an algorithm which does not make any distinction between augmented state variables.

Introducing  $\mathbf{T}$  in eq. (12) yields

$$\Delta \bar{\mathbf{z}} = \mathbf{B} \mathbf{H}^\top \mathbf{R}^{-1/2} \mathbf{T}^{-1} \mathbf{R}^{-1/2} (\mathbf{y} - \mathbf{H}(\bar{\mathbf{z}}^f)), \quad (14a)$$

$$\Delta \mathbf{X} = -\mathbf{B} \mathbf{H}^\top \mathbf{R}^{-1/2} (\mathbf{T} + \mathbf{T}^{1/2})^{-1} \mathbf{R}^{-1/2} \mathbf{H}(\mathbf{X}^f), \quad (14b)$$

where the linear algebra operators apply to symmetric matrices.

Finally, CL can be included in the analysis by replacing eq. (10) with

$$\mathbf{B} = \boldsymbol{\rho} \circ \left[ \mathbf{X}^f (\mathbf{X}^f)^\top \right], \quad (15)$$

where  $\boldsymbol{\rho} \in \mathbb{R}^{N_z \times N_z}$  is the localization matrix, a correlation matrix which depends on the geometry of all variables, and  $\circ$  is the Schur/Hadamard product. The resulting analysis is called the local EnSRF (LEnSRF).

In the following sections, we show how the EnSRF analysis (both global and local) can be efficiently implemented when the augmented state contains model parameters. In section 2.2.2, we only consider global model parameters, repeating (Bocquet *et al.*, 2020b), and in section 2.2.3, we consider the general case with both global and local model parameters.

### 2.2.2 The (local) EnSRF-ML analysis

Let us start with global parameters only (*i.e.*  $N_q = 0$ ). Following (Bocquet *et al.*, 2020b), it is possible to separate state and parameter update in the analysis to make it more efficient.

To do this, we split  $\mathbf{B}$  according to the state and parameter subspaces as in eq. (5). The ancillary matrix  $\mathbf{T}$  is equal to

$$\mathbf{T} = \mathbf{I} + \mathbf{R}^{-1/2} \mathbf{H}_x \mathbf{B}_{xx} \mathbf{H}_x^\top \mathbf{R}^{-1/2}. \quad (16)$$

Let us now introduce the additional ancillary variables  $\mathbf{u}_x \in \mathbb{R}^{N_x}$  and  $\mathbf{U}_x \in \mathbb{R}^{N_x \times N_e}$  defined as

$$\mathbf{u}_x \triangleq \mathbf{H}_x^\top \mathbf{R}^{-1/2} \mathbf{T}^{-1} \mathbf{R}^{-1/2} (\mathbf{y} - \mathbf{H}_x(\bar{\mathbf{x}}^f)), \quad (17a)$$

$$\mathbf{U}_x \triangleq -\mathbf{H}_x^\top \mathbf{R}^{-1/2} (\mathbf{T} + \mathbf{T}^{1/2})^{-1} \mathbf{R}^{-1/2} \mathbf{H}_x(\mathbf{X}_x^f). \quad (17b)$$

With these definitions, the mean update eq. (14a) becomes

$$\Delta \bar{\mathbf{x}} = \mathbf{B}_{xx} \mathbf{u}_x, \quad (18a)$$

$$\Delta \bar{\mathbf{p}} = \mathbf{B}_{px} \mathbf{u}_x, \quad (18b)$$

and the perturbation update eq. (14b) becomes

$$\Delta \mathbf{X}_x = \mathbf{B}_{xx} \mathbf{U}_x, \quad (19a)$$

$$\Delta \mathbf{X}_p = \mathbf{B}_{px} \mathbf{U}_x. \quad (19b)$$

Assuming that  $\mathbf{B}_{xx}$  is invertible, the parameter update formulae eqs. (18b) and (19b), can be written

$$\Delta \bar{\mathbf{p}} = \mathbf{B}_{px} \mathbf{B}_{xx}^{-1} \Delta \bar{\mathbf{x}}, \quad (20a)$$

$$\Delta \mathbf{X}_p = \mathbf{B}_{px} \mathbf{B}_{xx}^{-1} \Delta \mathbf{X}_x, \quad (20b)$$

which is the original parameter update derived by (Bocquet *et al.*, 2020b). Note that  $\mathbf{B}_{xx}^{-1}$  does not need to be computed since it applies to  $N_e \ll N_x$  vectors and only requires the solution of a linear system of equations with  $N_e N_x$  unknowns.

At this point, it is important to realize that the state update eqs. (18a) and (19a) is the usual EnSRF analysis while the parameter update eq. (20) is a regression of the state update into the parameter subspace. Such regression is very general and can be used regardless of the state update method. In our specific case however, the introduction of the ancillary variables  $\mathbf{u}_x$  and  $\mathbf{U}_x$  is an elegant way to bypass the matrix multiplication by  $\mathbf{B}_{xx}^{-1}$ . In a way, one can think of  $\mathbf{u}_x$  and  $\mathbf{U}_x$  as the uncorrelated increments. Moreover, note that the entire analysis does not depend on  $\mathbf{B}_{pp}$ .

When using CL, as for  $\mathbf{B}$ , we split  $\boldsymbol{\rho}$  in such a way that

$$\mathbf{B}_{xx} = \boldsymbol{\rho}_{xx} \circ \left[ \mathbf{X}_x^f (\mathbf{X}_x^f)^\top \right], \quad (21a)$$

$$\mathbf{B}_{px} = \boldsymbol{\rho}_{px} \circ \left[ \mathbf{X}_p^f (\mathbf{X}_x^f)^\top \right] = \mathbf{B}_{xp}^\top, \quad (21b)$$

$$\mathbf{B}_{pp} = \boldsymbol{\rho}_{pp} \circ \left[ \mathbf{X}_p^f (\mathbf{X}_p^f)^\top \right]. \quad (21c)$$

The localization matrix for the state subspace  $\rho_{xx}$  is the usual localization matrix. It almost certainly makes  $\mathbf{B}_{xx}$  positive definite, and in particular invertible. The localization matrix for the state-parameter cross subspace  $\rho_{px}$  has to be row-wise uniform because the parameters are global. Hence it is of the form

$$\rho_{px} = \text{diag}(\zeta_p)\mathbf{\Pi}_{px}, \quad (22)$$

where  $\mathbf{\Pi}_{px} \in \mathbb{R}^{N_p \times N_x}$  is the matrix full of ones and where  $\zeta_p \in \mathbb{R}^{N_p}$  is a vector of algorithmic parameters, one for each model parameter, which is more general than what was suggested in (Bocquet *et al.*, 2020b). Nonetheless, for the sake of simplicity, we choose in the following this vector to be uniform as in (Bocquet *et al.*, 2020b), such that  $\rho_{px} = \zeta_p \mathbf{\Pi}_{px}$ , where  $\zeta_p$  is a scalar algorithmic parameter. Looking at eqs. (18b) and (19b), we see that  $\zeta_p$  tapers the parameter update in a linear way: using  $\zeta_p = 1$  does not alter the parameter update while using  $\zeta_p = 0$  entirely disables the parameter update. For this reason,  $\zeta_p$  is called the *tapering* parameter. For simplicity and to emphasize the role of the tapering, we assume that  $\rho_{px} = \mathbf{\Pi}_{px}$  and we introduce  $\zeta_p$  directly into the parameter update, which is now written

$$\Delta \bar{\mathbf{p}} = \zeta_p \mathbf{B}_{px} \mathbf{u}_x, \quad (23a)$$

$$\Delta \mathbf{X}_p = \zeta_p \mathbf{B}_{px} \mathbf{U}_x. \quad (23b)$$

Finally, since  $\mathbf{B}_{pp}$  is not used during the analysis, we do not need to specify  $\rho_{pp}$ . Nevertheless, since the localization matrix  $\rho$  is by assumption a correlation matrix, it must be symmetric and positive definite. This means that the tapering parameter  $\zeta_p$  cannot take arbitrary values (Ruckstuhl and Janjić, 2018). See (Bocquet *et al.*, 2020b) for a detailed interpretation of  $\zeta_p$ .

For completeness, let us mention that the update eq. (20) is also valid without localization when  $\mathbf{B}_{xx}$  is not invertible (*i.e.* when  $N_e \leq N_x + 1$ ) provided that we replace the inverse by the Moore–Penrose pseudo-inverse. Indeed in this case, as proven in (Bocquet *et al.*, 2020b), the parameter update can be written

$$\Delta \bar{\mathbf{p}} = \mathbf{X}_p^f (\mathbf{X}_x^f)^+ \Delta \bar{\mathbf{x}}, \quad (24a)$$

$$\Delta \mathbf{X}_p = \mathbf{X}_p^f (\mathbf{X}_x^f)^+ \Delta \mathbf{X}_x, \quad (24b)$$

where the Moore–Penrose pseudo-inverse is indicated by a + superscript. Realizing that

$$\mathbf{X}_p^f (\mathbf{X}_x^f)^+ = \mathbf{X}_p^f (\mathbf{X}_x^f)^\top \left[ \mathbf{X}_x^f (\mathbf{X}_x^f)^\top \right]^+ = \mathbf{B}_{px} \mathbf{B}_{xx}^+, \quad (25)$$

we conclude that the update eq. (24) is equivalent to eq. (20) with the inverse replaced by the Moore–Penrose pseudo-inverse.

### 2.2.3 The (local) EnSRF-HML analysis

We now extend the EnSRF-ML analysis to the case where both global and local parameters are estimated. For this problem, we keep the state update and the global parameter update of the EnSRF-ML analysis, namely eqs. (18a), (19a) and (23), and we need to provide an update for the local parameters.

Following the arguments of section 2.2.2, we choose to write the local parameter update as

$$\Delta \bar{\mathbf{q}} = \mathbf{B}_{qx} \mathbf{u}_x, \quad (26a)$$

$$\Delta \mathbf{X}_q = \mathbf{B}_{qx} \mathbf{U}_x. \quad (26b)$$

Without localization, there is no distinction between local and global parameters. When using CL, in addition to eq. (21), we have

$$\mathbf{B}_{qx} = \rho_{qx} \circ \left[ \mathbf{X}_q^f (\mathbf{X}_x^f)^\top \right] = \mathbf{B}_{xq}^\top, \quad (27a)$$

$$\mathbf{B}_{qp} = \rho_{qp} \circ \left[ \mathbf{X}_q^f (\mathbf{X}_p^f)^\top \right] = \mathbf{B}_{pq}^\top, \quad (27b)$$

$$\mathbf{B}_{qq} = \rho_{qq} \circ \left[ \mathbf{X}_q^f (\mathbf{X}_q^f)^\top \right]. \quad (27c)$$

Again, since  $\mathbf{B}_{qp}$  and  $\mathbf{B}_{qq}$  are not used during the analysis, we do not need to specify  $\rho_{qp}$  and  $\rho_{qq}$ . The localization matrix for the state-local parameter cross subspace  $\rho_{qx}$  has to reflect the geometry of the local parameters and state variables, contrary to  $\rho_{px}$  which, as explained in section 2.2.2, has to be row-wise uniform. This point is important as  $\rho_{qx}$  is the only way to include localization in the local parameter update.

Finally, it is possible to normalize  $\rho_{qx}$  with its largest value:  $\rho_{qx} = \zeta_q \widehat{\rho}_{qx}$ . It turns out that  $\zeta_q$ , defined as the largest value of  $\rho_{qx}$ , has the same role in the local parameter update eq. (26) than the tapering parameter  $\zeta_p$  in the global

parameter update eqs. (18b) and (19b). Therefore, as in the previous section, we assume that  $\rho_{q_x} = \hat{\rho}_{q_x}$  and we introduce  $\zeta_q$  directly into the local parameter update, which is now written

$$\Delta \bar{q} = \zeta_q \mathbf{B}_{q_x} \mathbf{u}_x, \quad (28a)$$

$$\Delta \mathbf{X}_q = \zeta_q \mathbf{B}_{q_x} \mathbf{U}_x. \quad (28b)$$

Hereafter,  $\zeta_q$  is called the *local tapering* parameter, not to be confused with the (global) tapering parameter  $\zeta_p^2$ .

To conclude, the LEnSRF-HML analysis is summarized in [algorithm 1](#). By construction, it is equivalent to the generic LEnSRF analysis described in [section 2.2.1](#). In the limit where localization is disabled ( $\rho = \mathbf{I}$ , the matrix full of ones), the EnSRF-HML analysis is retrieved, and is equivalent to the generic EnSRF analysis described in [section 2.2.1](#).

---

#### Algorithm 1 LEnSRF-HML analysis

---

**Parameters:** localization matrices  $\rho_{xx}$  and  $\rho_{qx}$ , tapering parameters  $\zeta_p$  and  $\zeta_q$

**Input:** Forecast ensemble  $\mathbf{E}^f$

- 1:  $\bar{\mathbf{z}}^f = \mathbf{E}^f \mathbf{1} / N_e$
  - 2:  $\mathbf{X}^f = (\mathbf{E}^f - \bar{\mathbf{z}}^f \mathbf{1}^\top) / \sqrt{N_e - 1}$
  - 3:  $\mathbf{B}_{xx} = \rho_{xx} \circ \left[ \mathbf{X}_x^f (\mathbf{X}_x^f)^\top \right]$
  - 4:  $\mathbf{B}_{qx} = \rho_{qx} \circ \left[ \mathbf{X}_q^f (\mathbf{X}_x^f)^\top \right]$
  - 5:  $\mathbf{B}_{px} = \mathbf{X}_p^f (\mathbf{X}_x^f)^\top$
  - 6:  $\mathbf{T} = \mathbf{I} + \mathbf{R}^{-1/2} \mathbf{H}_x \mathbf{B}_{xx} \mathbf{H}_x^\top \mathbf{R}^{-1/2}$
  - 7:  $\mathbf{u}_x = \mathbf{H}_x^\top \mathbf{R}^{-1/2} \mathbf{T}^{-1} \mathbf{R}^{-1/2} (\mathbf{y} - \mathbf{H}_x (\bar{\mathbf{x}}^f))$
  - 8:  $\mathbf{U}_x = -\mathbf{H}_x^\top \mathbf{R}^{-1/2} (\mathbf{T} + \mathbf{T}^{1/2})^{-1} \mathbf{R}^{-1/2} \mathbf{H}_x (\mathbf{X}_x^f)$
  - 9:  $\Delta \bar{\mathbf{x}} = \mathbf{B}_{xx} \mathbf{u}_x$  ▷ state, mean update
  - 10:  $\Delta \bar{q} = \zeta_q \mathbf{B}_{q_x} \mathbf{u}_x$  ▷ local parameters, mean update
  - 11:  $\Delta \bar{p} = \zeta_p \mathbf{B}_{p_x} \mathbf{u}_x$  ▷ global parameters, mean update
  - 12:  $\Delta \mathbf{X}_x = \mathbf{B}_{xx} \mathbf{U}_x$  ▷ state, perturbation update
  - 13:  $\Delta \mathbf{X}_q = \zeta_q \mathbf{B}_{q_x} \mathbf{U}_x$  ▷ local parameters, perturbation update
  - 14:  $\Delta \mathbf{X}_p = \zeta_p \mathbf{B}_{p_x} \mathbf{U}_x$  ▷ global parameters, perturbation update
  - 15: **return**  $\mathbf{E}^a = (\bar{\mathbf{z}}^f + \Delta \bar{\mathbf{z}}) \mathbf{1}^\top + \sqrt{N_e - 1} (\mathbf{X}^f + \Delta \mathbf{X})$  ▷ Analysis ensemble
- 

### 2.3 The ensemble transform Kalman filter

We now focus on the EnKFs with DL, for which the local ETKF (LETKF) is the archetype.

#### 2.3.1 The generic (local) ETKF analysis

The generic ETKF analysis is given by the following set of equations:

$$\Delta \bar{\mathbf{z}} = \mathbf{X}^f \mathbf{w}^a, \quad (29a)$$

$$\Delta \mathbf{X} = \mathbf{X}^f (\mathbf{T}^{-1/2} - \mathbf{I}). \quad (29b)$$

Equation (29a) is known as the mean update and eq. (29b) as the perturbation update. In these equations,  $\mathbf{Y} \in \mathbb{R}^{N_y \times N_e}$ ,  $\mathbf{T} \in \mathbb{R}^{N_e \times N_e}$ , and  $\mathbf{w}^a \in \mathbb{R}^{N_e}$  are ancillary variables defined by

$$\mathbf{Y} \triangleq \mathbf{H} (\mathbf{X}^f), \quad (30a)$$

$$\mathbf{T} \triangleq \mathbf{I} + \mathbf{Y}^\top \mathbf{R}^{-1} \mathbf{Y}, \quad (30b)$$

$$\mathbf{w}^a \triangleq \mathbf{T}^{-1} \mathbf{Y}^\top \mathbf{R}^{-1} (\mathbf{y} - \mathbf{H} (\bar{\mathbf{z}}^f)). \quad (30c)$$

The main advantage of the ETKF analysis is that the linear algebra is expressed in the ensemble space ( $\mathbb{R}^{N_e}$ ), which is usually much smaller than both the observation number and the augmented state space dimension ( $N_e \ll N_y, N_z$ ).

---

<sup>2</sup>For completeness, we mention that, once again, it is possible to use a vector algorithmic parameter  $\zeta_q$  instead of the scalar algorithmic parameter  $\zeta_q$ , but we chose not to for the sake of simplicity.

Unfortunately, CL, expressed in the augmented state space, cannot be used in the analysis. Nevertheless, DL can be included in the ETKF by making the analysis local following (Hunt *et al.*, 2007; Neger and Gregg, 2007).

For each augmented state variable  $n \in \{1, \dots, N_z\}$ , the inverse of the observation error covariance is tapered:

$$\mathbf{R}_n^{-1} \triangleq \boldsymbol{\rho}_n \circ \mathbf{R}^{-1}, \quad (31)$$

where  $\boldsymbol{\rho}_n \in \mathbb{R}^{N_y \times N_y}$  is the localization matrix in observation space for the  $n$ -th variable, a correlation matrix, which depends on the geometry of the observations relative to the  $n$ -th variable. This yields local variants of  $\mathbf{T}$  and  $\mathbf{w}^a$  which are used to compute the  $n$ -th row of the mean and perturbation updates  $\Delta \bar{\mathbf{z}}$  and  $\Delta \mathbf{X}$ . This describes the LETKF analysis. By construction, the localization matrix  $\boldsymbol{\rho}_n$  is rigorously defined only when both the observations and the  $n$ -th variable are local.

A key asset of the ETKF is that eq. (29), which describes the generic ETKF analysis, can also be used to implement the ETKF-ML analysis in a very efficient way. By contrast, the generic LETKF analysis described above cannot be used to implement the LETKF-ML analysis because the localization matrix  $\boldsymbol{\rho}_n$  cannot be rigorously defined for global model parameters.

Therefore, in the following sections, we derive an equivalent update for the ETKF-ML analysis. The goal is to provide an update scheme equivalent to eq. (29) in the global case while being generalizable to DL with global model parameters. In section 2.3.2, we only consider global model parameters, repeating and improving upon (Bocquet *et al.*, 2020b), and in section 2.3.3, we consider the general case with both global and local model parameters.

### 2.3.2 The (local) ETKF-ML analysis

Let us start with global parameters only (*i.e.*  $N_q = 0$ ). Following (Bocquet *et al.*, 2020b), it is possible to separate state and parameter update in the analysis. The state update is performed using the same ensemble transform as in the generic ETKF:

$$\Delta \bar{\mathbf{x}} = \mathbf{X}_x^f \mathbf{w}^a, \quad (32a)$$

$$\Delta \mathbf{X}_x = \mathbf{X}_x^f \left( \mathbf{T}^{-1/2} - \mathbf{I} \right), \quad (32b)$$

and the parameter update is performed using the pseudo-inverse formulae eq. (24), which we recall here:

$$\Delta \bar{\mathbf{p}} = \mathbf{X}_p^f \left( \mathbf{X}_x^f \right)^+ \Delta \bar{\mathbf{x}}, \quad (33a)$$

$$\Delta \mathbf{X}_p = \mathbf{X}_p^f \left( \mathbf{X}_x^f \right)^+ \Delta \mathbf{X}_x. \quad (33b)$$

When enforcing DL, the state update eq. (32) is made local (following the method described in section 2.3.1), while the parameter update eq. (33) is only indirectly localized. Indeed, as explained in section 2.2.2, the parameter update is a regression of the state update eq. (32), which is localized, to the parameter subspace. This update, combined with the state update eq. (32), defines the LETKF-ML analysis as originally proposed in (Bocquet *et al.*, 2020b).

However, eq. (25) shows that without localization,  $\mathbf{X}_p^f \left( \mathbf{X}_x^f \right)^+$  is equal to  $\mathbf{B}_{px} \mathbf{B}_{xx}^+$  which, with CL, becomes  $\mathbf{B}_{px} \mathbf{B}_{xx}^{-1}$  where  $\mathbf{B}_{xx}$  has been localized with  $\boldsymbol{\rho}_{xx}$ . This last localization footprint is missing in the original LETKF-ML analysis in (Bocquet *et al.*, 2020b); we have numerically checked that, although working as expected, it makes the LETKF-ML distinctively not as accurate as the LEnSRF-ML algorithm. To fix this issue, we propose a more consistent approach for the parameter update.

Instead of using the pseudo-inverse formulae eq. (33), we propose to use the parameter update of the EnSRF-ML analysis, namely eqs. (18b) and (19b) which we recall here:

$$\Delta \bar{\mathbf{p}} = \mathbf{X}_p^f \left( \mathbf{X}_x^f \right)^\top \mathbf{u}_x, \quad (34a)$$

$$\Delta \mathbf{X}_p = \mathbf{X}_p^f \left( \mathbf{X}_x^f \right)^\top \mathbf{U}_x, \quad (34b)$$

where the uncorrelated increments  $\mathbf{u}_x$  and  $\mathbf{U}_x$ , originally defined by eq. (17), can be rewritten using the ancillary variables of the ETKF  $\mathbf{Y}$ ,  $\mathbf{T}$ , and  $\mathbf{w}^a$  defined by eq. (30):

$$\mathbf{u}_x = \mathbf{H}_x^\top \mathbf{R}^{-1} \left( \mathbf{y} - \mathbf{H}_x \left( \bar{\mathbf{x}}^f \right) - \mathbf{Y} \mathbf{w}^a \right), \quad (35a)$$

$$\mathbf{U}_x = -\mathbf{H}_x^\top \mathbf{R}^{-1} \mathbf{Y} \left( \mathbf{T} + \mathbf{T}^{1/2} \right)^{-1}. \quad (35b)$$

This parameter update, combined with the state update [eq. \(32\)](#), defines the ETKF-ML analysis used in this paper. A proof of these formulae can be found in [appendix A](#).

Enforcing DL in the parameter update of this new ETKF-ML analysis is straightforward. First, the construction of the uncorrelated increments  $\mathbf{u}_x$  and  $\mathbf{U}_x$  with [eq. \(35\)](#) is made local (following the method described in [section 2.3.1](#)), and then the parameter update is computed (globally) with [eq. \(34\)](#). The resulting LETKF-ML analysis has exactly the same amount of localization footprints as the LEnSRF-ML analysis. Furthermore, since there is a one-to-one correspondence between the rows of  $\mathbf{x}$  and  $\mathbf{X}_x$  and those of  $\mathbf{u}_x$  and  $\mathbf{U}_x$ , the local variants of [eqs. \(32\)](#) and [\(35\)](#) can be computed inside the same localization loop. However, we recall that this scheme assumes that the observations are local. Nevertheless, it improves upon the approximate technique proposed in ([Aksoy et al., 2006](#)) as it makes the update seemingly rigorous.

Finally, as proposed in ([Bocquet et al., 2020b](#)) and taking again inspiration from the EnSRF-ML analysis, it is possible to taper the parameter update and hence to replace [eq. \(34\)](#) by

$$\Delta \bar{\mathbf{p}} = \zeta_p \mathbf{X}_p^f (\mathbf{X}_x^f)^\top \mathbf{u}_x, \quad (36a)$$

$$\Delta \mathbf{X}_p = \zeta_p \mathbf{X}_p^f (\mathbf{X}_x^f)^\top \mathbf{U}_x, \quad (36b)$$

where  $\zeta_p$  is the global tapering parameter. In the EnSRF-ML analysis, the values of  $\zeta_p$  are bounded by the fact that they are used in the definition of a positive definite matrix. By contrast here, there is no such constraint and  $\zeta_p$  can take arbitrary values.

### 2.3.3 The (local) ETKF-HML analysis

We now extend the ETKF-ML analysis to the case where we have both global and local parameters to estimate. For this problem, we keep the state update and the global parameter update of the ETKF-ML analysis, namely [eqs. \(32\)](#) and [\(36\)](#), and we need to provide an update for the local parameters.

We choose to perform the local parameter update using the same ensemble transform as in the generic ETKF, with the addition of the local tapering parameter:

$$\Delta \bar{\mathbf{q}} = \zeta_q \mathbf{X}_q^f \mathbf{w}^a, \quad (37a)$$

$$\Delta \mathbf{X}_q = \zeta_q \mathbf{X}_q^f (\mathbf{T}^{-1/2} - \mathbf{I}). \quad (37b)$$

This update, combined with the state update [eq. \(32\)](#) and the global parameter update [eq. \(36\)](#), defines the ETKF-HML analysis. The local tapering parameter  $\zeta_q$  enables a full similarity between the ETKF-HML and EnSRF-HML analyses.

Enforcing DL in this ETKF-HML is straightforward: the local parameter update is made local following the method described in [section 2.3.1](#). Note however, that even though the local parameters are local, their geometry may differ from the geometry of the state variables. Therefore, a rigorous definition of the LETKF-HML analysis could require two set of localization matrices:  $\{\rho_n^x, n = 1, \dots, N_x\}$  for the state variables and  $\{\rho_m^q, m = 1, \dots, N_q\}$  for the local parameters. Hence the local state updates and local parameter updates are computed in two different localization loops. If the geometry of the local parameters coincides with that of the state variables, then the two localization loops can potentially be merged.

To conclude, the LETKF-HML analysis is summarized in [algorithm 2](#). In the limit where localization is disabled (for all  $n \in \{1, \dots, N_x\}$ , and  $m \in \{1, \dots, N_q\}$ ,  $\rho_n^x = \rho_m^q = \mathbf{1}$ , the matrix full of ones), one recovers the ETKF-HML analysis, which is equivalent to the generic ETKF analysis described in [section 2.3.1](#). Furthermore, the generic ETKF analysis being equivalent to the generic EnSRF analysis, we conclude that the ETKF-HML analysis is equivalent to the EnSRF-HML analysis. However, even though the LEnSRF-HML analysis is equivalent to the generic LEnSRF analysis, the LETKF-HML analysis is not equivalent to the generic LETKF analysis which is not defined (because of the global parameters). Finally, the parameter localization is somewhat similar between the LETKF-HML and the LEnSRF-HML analyses, which is why we expect the difference in performance between the LETKF-HML and the LEnSRF-HML algorithms to be of the same order as the difference in performance between the LETKF and the LEnSRF algorithms ([Sakov and Bertino, 2011](#)).

The algorithms presented in [section 2.2](#) and [section 2.3](#) are summarized in [table 4](#).

## 3 Illustration of the EnKF-ML algorithms with a 1D model

In this section, the EnKF-HML family of algorithms are illustrated numerically using the Lorenz 1996 (L96) model ([Lorenz and Emanuel, 1998](#)). The standard L96 model with 40 variables is widely used in DA to test new methods, but we choose here to use an inhomogeneous variant to illustrate the need for local parameters.

**Algorithm 2** LETKF-HML analysis

---

**Parameters:** localization matrices  $\{\rho_n^x, n = 1, \dots, N_x\}$  and  $\{\rho_m^q, m = 1, \dots, N_q\}$ , tapering parameters  $\zeta_p$  and  $\zeta_q$

**Input:** Forecast ensemble  $\mathbf{E}^f$

- 1:  $\bar{\mathbf{z}}^f = \mathbf{E}^f \mathbf{1} / N_e$
- 2:  $\mathbf{X}^f = (\mathbf{E}^f - \bar{\mathbf{z}}^f \mathbf{1}^\top) / \sqrt{N_e - 1}$
- 3:  $\mathbf{Y} = \mathbf{H}_x (\mathbf{X}^f)$
- 4: **for**  $n = 1$  **to**  $N_x$  **do**
- 5:    $\mathbf{R}_n^{-1} = \rho_n^x \circ \mathbf{R}^{-1}$
- 6:    $\mathbf{T}_n = \mathbf{I} + \mathbf{Y}^\top \mathbf{R}_n^{-1} \mathbf{Y}$
- 7:    $\mathbf{w}_n^a = \mathbf{T}_n^{-1} \mathbf{Y}^\top \mathbf{R}_n^{-1} (\mathbf{y} - \mathbf{H}_x (\bar{\mathbf{x}}^f))$
- 8:    $[\mathbf{u}_x]_n = [\mathbf{H}_x^\top \mathbf{R}_n^{-1} (\mathbf{y} - \mathbf{H}_x (\bar{\mathbf{x}}^f)) - \mathbf{Y} \mathbf{w}_n^a]_n$
- 9:    $[\mathbf{U}_x]_{n,:} = \left[ -\mathbf{H}_x^\top \mathbf{R}_n^{-1} \mathbf{Y} (\mathbf{T}_n + \mathbf{T}_n^{1/2})^{-1} \right]_{n,:}$
- 10:    $[\Delta \bar{\mathbf{x}}]_n = [\mathbf{X}_x^f \mathbf{w}_n^a]_n$   $\triangleright$  state, mean update [local]
- 11:    $[\Delta \mathbf{X}_x]_{n,:} = [\mathbf{X}_x^f (\mathbf{T}_n^{-1/2} - \mathbf{I})]_{n,:}$   $\triangleright$  state, perturbation update [local]
- 12: **end for**
- 13: **for**  $m = 1$  **to**  $N_q$  **do**
- 14:    $\mathbf{R}_m^{-1} = \rho_m^q \circ \mathbf{R}^{-1}$
- 15:    $\mathbf{T}_m = \mathbf{I} + \mathbf{Y}^\top \mathbf{R}_m^{-1} \mathbf{Y}$
- 16:    $\mathbf{w}_m^a = \mathbf{T}_m^{-1} \mathbf{Y}^\top \mathbf{R}_m^{-1} (\mathbf{y} - \mathbf{H}_x (\bar{\mathbf{x}}^f))$
- 17:    $[\Delta \bar{\mathbf{q}}]_m = \zeta_q [\mathbf{X}_q^f \mathbf{w}_m^a]_m$   $\triangleright$  local parameters, mean update [local]
- 18:    $[\Delta \mathbf{X}_q]_{m,:} = \zeta_q [\mathbf{X}_q^f (\mathbf{T}_m^{-1/2} - \mathbf{I})]_{m,:}$   $\triangleright$  local parameters, perturbation update [local]
- 19: **end for**
- 20:  $\Delta \bar{\mathbf{p}} = \zeta_p \mathbf{X}_p^f (\mathbf{X}_x^f)^\top \mathbf{u}_x$   $\triangleright$  global parameters, mean update
- 21:  $\Delta \mathbf{X}_p = \zeta_p \mathbf{X}_p^f (\mathbf{X}_x^f)^\top \mathbf{U}_x$   $\triangleright$  global parameters, perturbation update
- 22: **return**  $\mathbf{E}^a = (\bar{\mathbf{z}}^f + \Delta \bar{\mathbf{z}}) \mathbf{1}^\top + \sqrt{N_e - 1} (\mathbf{X}^f + \Delta \mathbf{X})$   $\triangleright$  Analysis ensemble

---

**3.1 The inhomogeneous Lorenz 1996 model**

The L96 model is defined by a set of ODEs over a periodic domain with  $N_x$  variables, indexed by  $n = 1, \dots, N_x$ :

$$\frac{dx_n}{dt} = (x_{n+1} - x_{n-2})x_{n-1} - x_n + F, \quad (38)$$

where  $F$  is the forcing coefficient and  $x_1 = x_{N_x+1}$ ,  $x_0 = x_{N_x}$ , and  $x_{-1} = x_{N_x-1}$  to ensure periodicity. The inhomogeneous L96 (L96i) model is a variant of the L96 model in which the constant forcing  $F$  is replaced by a local forcing  $F_n$  which depends on the state variable index  $n$ .

The standard L96 model uses  $N_x = 40$  variables and  $F = 8$ . For our experiments we use the L96i model with  $N_x = 40$  variables as well and the local forcing is defined as

$$F_n \triangleq 8 + \cos\left(\frac{2\pi n}{N_x}\right). \quad (39)$$

The model is integrated using a fourth-order Runge–Kutta scheme with a time step of  $\delta t = 0.05$ . We checked that it has 13 positive Lyapunov exponents and a neutral one, yielding an unstable-neutral subspace of dimension 14.

**3.2 The surrogate model**

As explained in the beginning of [section 2](#), the EnKF-HML algorithms do not use the true model for the forecast but a surrogate model instead, whose parameters are estimated during the analysis. Following ([Bocquet et al., 2020a,b](#)), we choose to use the surrogate model designed in ([Bocquet et al., 2019](#)). In this model, the tendencies are parameterized by a set of regressors called the *monomials*, and are then integrated in time to build the resolvent between two time steps. This model can in principle represent any homogeneous ODE, provided that the number of monomials (which is determined by  $L$ , the size of the local *stencil*) is sufficient. See ([Bocquet et al., 2019](#)) for more details about the implementation.

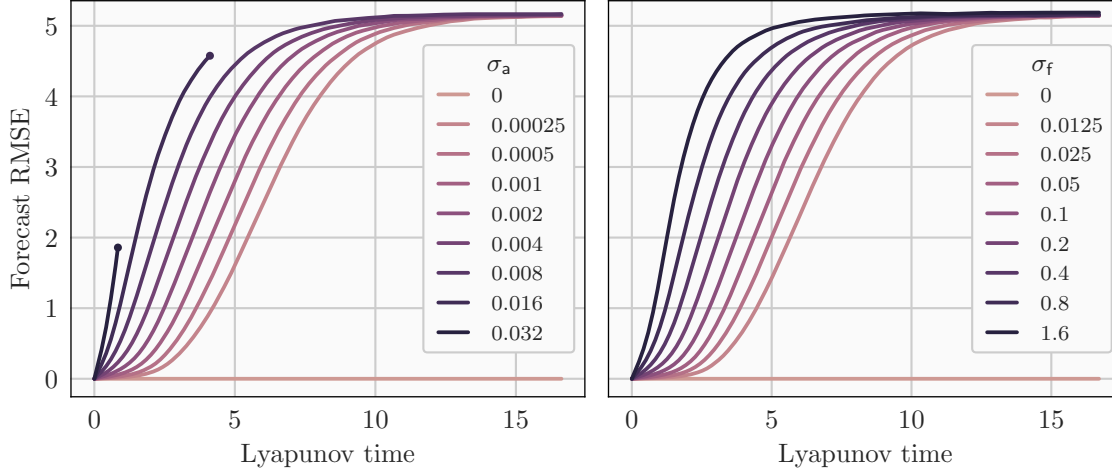


Figure 1: Forecast skill of the surrogate model  $\text{sur}(\mathbf{a}, \mathbf{f})$  compared to  $\text{sur}(\mathbf{a}^t, \mathbf{f}^t)$ , the true L96i model. Left panel:  $\mathbf{f} = \mathbf{f}^t$  and  $\mathbf{a} = \mathbf{a}^t + \mathbf{a}'$  with  $\mathbf{a}' \sim \mathcal{N}(0, \sigma^2 \mathbf{I})$  for increasing  $\sigma$ . Right panel:  $\mathbf{a} = \mathbf{a}^t$  and  $\mathbf{f} = \mathbf{f}^t + \mathbf{f}'$  with  $\mathbf{f}' \sim \mathcal{N}(0, \sigma^2 \mathbf{I})$  for increasing  $\sigma$ . Each experiment is repeated 5000 times, with different parameter perturbations and different initial conditions. The curves are stopped with a dot when at least one of the 5000 repetitions diverged.

In our experiments, we use a stencil of  $L = 2$ , we replace the global forcing coefficient by local forcing coefficients, and we use a fourth-order Runge–Kutta scheme with a time step of  $\delta t = 0.05$  to integrate the tendencies. The surrogate model is defined on  $N_x = 40$  state variables, in a one-to-one correspondence with those of the L96i, and has a total of  $\frac{3}{2}(L+1) \times (L+2) - 1 + N_x = 17 + 40 = 57$  parameters. The first 17 parameters correspond to linear and bilinear monomial coefficients. The other 40 parameters correspond to the local forcing coefficients. For convenience, we introduce  $\text{sur}(\mathbf{a}, \mathbf{f})$  as the surrogate model in which the 17 monomial coefficients are in vector  $\mathbf{a}$  and the 40 forcing coefficients are in vector  $\mathbf{f}$ .

By construction, it is possible to reproduce the L96i model with a specific set of parameters which we write  $\mathbf{a}^t$  and  $\mathbf{f}^t$ :  $\text{sur}(\mathbf{a}^t, \mathbf{f}^t)$  is the L96i model. The values of  $\mathbf{a}^t$  lie in  $\{-1, 0, 1\}$  while the values of  $\mathbf{f}^t$  are given by eq. (39). The sensitivity of the surrogate model  $\text{sur}(\mathbf{a}, \mathbf{f})$  to  $\mathbf{a}$  and  $\mathbf{f}$  is illustrated in fig. 1 using the forecast skill, which is defined as the average integration error after a given lead time starting from the correct initial condition.

### 3.3 Experimental setup

#### 3.3.1 The inference problem

The experiments consist in twin simulations. The truth is generated using the L96i model, or equivalently using  $\text{sur}(\mathbf{a}^t, \mathbf{f}^t)$ . The system is fully observed,  $\mathbf{H}_x(\mathbf{x}) = \mathbf{x}$ , with a period of  $\Delta t = 0.05$ , and the observations are independently perturbed with a normal distribution of error covariance matrix  $\mathbf{R} = \mathbf{I}$ .

Three categories of experiments are performed, with an increasing number of parameters to estimate alongside the state.

1. In the first category, the goal is to estimate the 17 monomial coefficients  $\mathbf{a}$ . This inference problem is very similar to the one considered in (Bocquet *et al.*, 2020b).
2. In the second category, the goal is to estimate the 40 forcing coefficients  $\mathbf{f}$ .
3. In the third category, the goal is to estimate all 57 coefficients.

In all experiments, the main performance metric is the time-averaged root mean squared error (RMSE) of the state analysis. In such cycled experiments, small RMSE scores for the state estimation can only be obtained with accurate models, which is why most of the time we do not report the parameter RMSE. Furthermore, the exact numbers of spin-up and assimilation cycles depend on the experiment and are specified later.

#### 3.3.2 Tested algorithms

Our objective is to implement and test the LETKF-HML and LEnSRF-HML algorithms, for which we need to specify the set of global and local parameters  $\mathbf{p}$  and  $\mathbf{q}$  to be estimated alongside the state. The 17 monomial coefficients  $\mathbf{a}$  affect

Table 2: Setup for the different algorithmic variants tested in [section 3.4](#). For each experiment, we specify the inference problem (first column), the analysis algorithm (second column), the forecast model (third column), the definition of the set of global and local coefficients (fourth and fifth columns) and their numbers (sixth and seventh columns).

Inference problem	Algorithm	Model	$\mathbf{p}$	$\mathbf{q}$	$N_p$	$N_q$
1: $(\mathbf{x}, \mathbf{a})$	LEnSRF-ML	sur $(\mathbf{a}, \mathbf{f}^t)$	$\mathbf{a}$		17	
	LETKF-ML	sur $(\mathbf{a}, \mathbf{f}^t)$	$\mathbf{a}$		17	
	LETKF-Aksoy	sur $(\mathbf{a}, \mathbf{f}^t)$	$\mathbf{a}$		17	
2: $(\mathbf{x}, \mathbf{f})$	LETKF-ML	sur $(\mathbf{a}^t, \mathbf{f})$		$\mathbf{f}$	40	
	LETKF-LML	sur $(\mathbf{a}^t, \mathbf{f})$		$\mathbf{f}$		40
3: $(\mathbf{x}, \mathbf{a}, \mathbf{f})$	LETKF-HML	sur $(\mathbf{a}, \mathbf{f})$	$\mathbf{a}$	$\mathbf{f}$	17	40
	LEnSRF-HML	sur $(\mathbf{a}, \mathbf{f})$	$\mathbf{a}$	$\mathbf{f}$	17	40

the model tendencies in a global way. Therefore, if they need to be estimated, they must be included in the set of global parameters  $\mathbf{p}$ . By contrast, the 40 forcing coefficients  $\mathbf{f}$  affect the model tendencies locally. This means that, if they need to be estimated, they can be included either in the set of global parameters  $\mathbf{p}$  (*i.e.*, ignoring their local nature) or in the set of local parameters  $\mathbf{q}$ . In order to distinguish the different algorithmic variants, we will replace the -HML suffix by a -ML suffix when there are only global parameters to estimate ( $N_q = 0$ ) and by a -LML suffix when there are only local parameters to estimate ( $N_p = 0$ ). This terminology is consistent with the definition of the EnKF-ML algorithms.

For comparison, we also implement and test the algorithm of (Aksoy *et al.*, 2006), hereafter called LETKF-Aksoy. This is a variant of the LETKF suited for parameter estimation, in which the global parameter update is performed through an empirical averaging of local updates.

The setup for all the LEnKF-HML variants tested in [section 3.4](#) is summarized in [table 2](#).

### 3.3.3 Ensemble initialization

As shown in (Bocquet *et al.*, 2020b), the ensemble initialization may have an impact on the time-averaged metric (even with a very long run). In this paper, this is less critical because we only use localized ensemble DA algorithms. Nevertheless, we stick to the initialization method as in (Bocquet *et al.*, 2020b). Namely, the  $i$ -th ensemble member is initialized as

$$\mathbf{z}_i = \mathbf{z}^\dagger + \mathbf{z}' + \mathbf{z}''_i, \quad \mathbf{z}', \mathbf{z}''_i \sim \mathcal{N}(\mathbf{0}, \Sigma), \quad (40)$$

where  $\mathbf{z}^\dagger$  is the true initial state,  $\mathbf{z}'$  is the initial bias, and  $\mathbf{z}''_i$  is the  $i$ -th anomaly. The covariance matrix  $\Sigma$  is diagonal, equal to 1 for the state variables and to 0.2 for both the local and global parameters. As shown in [fig. 1](#), having a 0.2 bias in the parameters is sufficient to make the surrogate model really inaccurate.

### 3.3.4 Algorithm parameterization

For the LEnSRF-HML analysis, [algorithm 1](#), we need to specify two localization matrices: the classical localization matrix between state variables,  $\rho_{xx}$ , and the cross localization matrix between state variables and local parameters  $\rho_{qx}$ . In all our experiments, the geometry<sup>3</sup> of the local parameters (if any) is the same as the geometry of the state variables. Therefore, we enforce  $\rho_{qx} = \rho_{xx}$  and  $\rho_{xx}$  is chosen as

$$[\rho_{xx}]_{mn} \triangleq \text{GC} \left( \frac{2d(m, n)}{r} \right), \quad (41)$$

where GC is the Gaspari–Cohn piecewise rational function (Gaspari and Cohn, 1999),  $d(m, n)$  is the (circular) distance between the  $m$ -th and  $n$ -th variables, and  $r$  is the localization radius, the only algorithmic parameter relative to localization.

For the LETKF-HML analysis, [algorithm 2](#), we also need to specify two sets of localization matrices: the classical localization matrices between observations and state variables,  $\rho_n^x$ , and the localization matrices between observations and local parameters,  $\rho_n^q$ . For the same reasons as above, we enforce  $\rho_n^q = \rho_n^x$  and the  $\rho_n^x$  matrices are chosen as

$$[\rho_n^x]_{ij} \triangleq \sqrt{\text{GC} \left( \frac{2d(i, n)}{r} \right) \text{GC} \left( \frac{2d(j, n)}{r} \right)}, \quad (42)$$

<sup>3</sup>By geometry, we mean here the number of variables and their position in space.

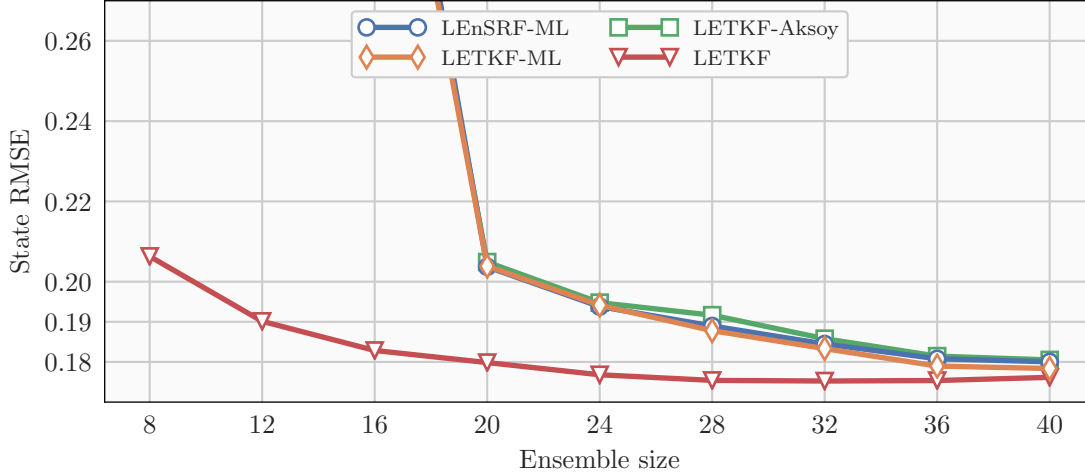


Figure 2: Time-averaged state analysis RMSE as a function of the ensemble size  $N_e$  for the first test series (estimation of the 17 monomial coefficients  $\mathbf{a}$ ) with the LEnSRF-ML (in blue), the LETKF-ML (in yellow), and the LETKF-Aksoy (in green). For reference, the red line shows the scores obtained with the LETKF when the model is known.

where  $d(i, n)$  and  $d(j, n)$  are the distances between the  $i$ -th observation and the  $n$ -th variable and between the  $j$ -th observation and the  $n$ -th variable, respectively, and  $r$  is the localization radius. Besides, having the same geometry for the state variables and the local parameters means that the two for-loops in [algorithm 2](#) can be merged.

Finally, in order to mitigate the sampling errors, we use a multiplicative inflation on the prior with a uniform and constant in time coefficient  $\lambda$ .

To summarize, our algorithms depend on at most four scalar parameters: the localization radius  $r$  (which parameterizes the Gaspari–Cohn function), the inflation coefficient  $\lambda$ , and the two tapering coefficients  $\zeta_p$  and  $\zeta_q$  introduced in [section 2](#). Unless otherwise mentioned, each algorithmic parameter is optimally tuned to yield the lowest state RMSE.

### 3.4 Results

In this section, we present the results of our numerical experiments, organized according to the classification described in [section 3.3.1](#).

#### 3.4.1 Estimation of the 17 monomial coefficients

In this first test series, the goal is to estimate the 17 monomial coefficients  $\mathbf{a}$  only. As explained in [section 3.3.2](#), these coefficients affect the model tendencies in a global way, and hence must be included in the set of global parameters  $\mathbf{p}$ , which means that  $N_p = 17$ . For these experiments, there is no local parameters:  $N_q = 0$ . The setup for each LEnKF-HML variant tested in this section is recalled in [table 2](#) (first three rows).

There are only two minor differences between this inference problem and the one considered in ([Bocquet et al., 2020b](#)). First, the truth is generated using the L96i model and not the L96 model. Second, the number of parameters  $N_p$  to estimate is 17 and not 18. Indeed, the inference problem of ([Bocquet et al., 2020b](#)) also included a global forcing coefficient. This global forcing coefficient has been replaced by the local forcing coefficients  $\mathbf{f}$  (while defining the L96i model) which are not estimated in this first test series.

The results are shown in [fig. 2](#). The state analysis RMSE is averaged over 3000 cycles after a spin-up period of 3000 cycles, and over 8 repetitions of the experiments. This is empirically sufficient to ensure the convergence of the statistical indicators.

As expected from the similarity between the inference problems, the scores obtained with the LEnSRF-ML are overall similar to those reported by ([Bocquet et al., 2020b](#)). The minimal ensemble size  $N_e$  for a successful run (analysis RMSE around 0.2) is 20. This corresponds to 17 members for the  $N_p = 17$  global parameters (each global parameter is a neutral mode of the dynamics) plus a few additional members for the  $N_x = 40$  state variables, for which the number of unstable and neutral modes is 14, but which benefit from localization.

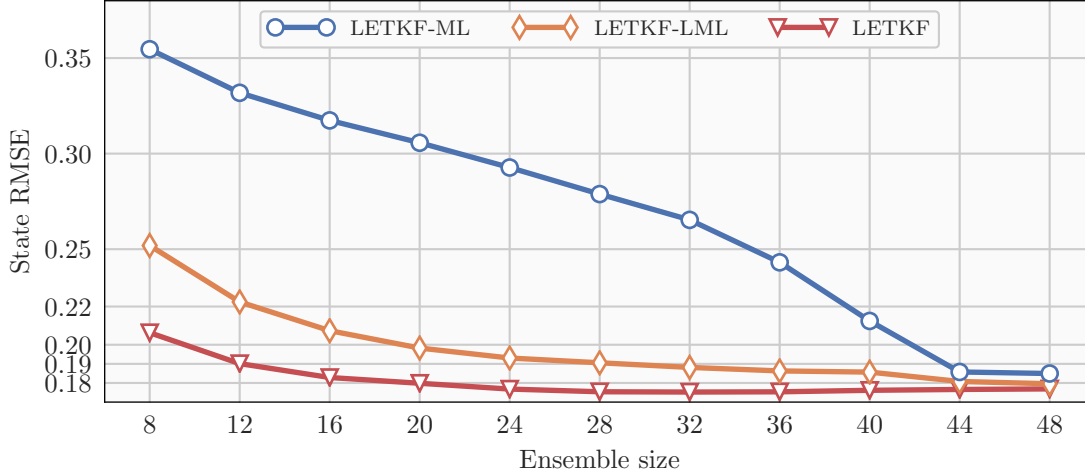


Figure 3: Time-averaged state analysis RMSE as a function of the ensemble size  $N_e$  for the second test series (estimation of the 40 forcing coefficients  $\mathbf{f}$ ) with the LETKF-ML (in blue) and the LETKF-LML (in yellow). For reference, the red line shows the scores obtained with the LETKF when the forcing coefficients are known.

There is almost no difference between the scores of the LEnSRF-ML and those of the LETKF-ML. This is not a surprise because the global parameter update of the LETKF-ML has been redesigned in [section 2.3.2](#) to mimic that of the LEnSRF-ML, in such a way that the LEnSRF-ML and the LETKF-ML are as close to another as the LEnSRF and the LETKF.

More suprisingly, the LETKF-Aksoy method yields very similar results although for this algorithm, the global parameters are updated by computing the average of local updates, which *seems* less rigorous as the global parameter update of the LEnKF-ML algorithms. A further study is required to understand the mathematical justification of the global parameter update of the LETKF-Aksoy (for example using the alternating direction method of multipliers method, see ([Boyd et al., 2011](#)) and references therein) and its potential limitations.

Finally, even though  $N_e = 20$  members are sufficient for a successful run, there is still at this point a small gap between the scores of the LEnKF-ML algorithms (*i.e.* with parameter estimation) and those of the LETKF (*i.e.* with known model). According to ([Bocquet et al., 2020b](#)), this gap comes from the use of a uniform (rather than adaptive) inflation and indeed progressively vanishes as the ensemble size  $N_e$  grows.

### 3.4.2 Estimation of the 40 forcing coefficients

In this second test series, the goal is to estimate the 40 forcing coefficients  $\mathbf{f}$  only. As explained in [section 3.3.2](#), these coefficients affect the model tendencies in a local way, and hence they can be included either in the set of global parameters  $\mathbf{p}$  or in the set of local parameters  $\mathbf{q}$ . Our objective is to compare the two approaches and demonstrate that parameter localization is effective. The setup for each LEnKF-HML variant tested in this section is recalled in [table 2](#) (fourth and fifth rows).

The results are shown in [fig. 3](#). The state analysis RMSE is averaged over 3000 cycles after a spin-up period of 5000 cycles, and over 8 repetitions of the experiments.

With the LETKF-ML, the local nature of the forcing coefficients  $\mathbf{f}$  is ignored and hence the algorithm uses  $N_p = 40$  global parameters and no local parameters:  $N_q = 0$ . As in the previous test series, we expect that the minimal ensemble size  $N_e$  for a successful run should be around  $N_p = 40$  members for the global parameters (each global parameter is a neutral mode of the dynamics) plus a few additional members for the  $N_x = 40$  state variables, for which the number of unstable and neutral modes is 14, but which benefit from the localization. This is indeed what is observed in [fig. 3](#). However, the divergence of the LETKF-ML for small ensembles ( $N_x \leq 40$ ) is much less pronounced here than in the first test series. This can be explained by the fact that the surrogate model  $\text{sur}(\mathbf{a}, \mathbf{f})$  is more sensitive to a perturbation of the monomial coefficients  $\mathbf{a}$  than to a perturbation of the forcing coefficients  $\mathbf{f}$ , as illustrated by [fig. 1](#). In particular, the initial bias in model parameters (as described in [section 3.3.3](#)) is much weaker in relative terms in this test series than in the first one.

With the LETKF-LML, the local nature of the forcing coefficients  $\mathbf{f}$  is fully exploited. Hence the algorithm uses  $N_q = 40$  local parameters and no global parameters:  $N_p = 0$ . [Figure 3](#) shows that the localization of the parameters is

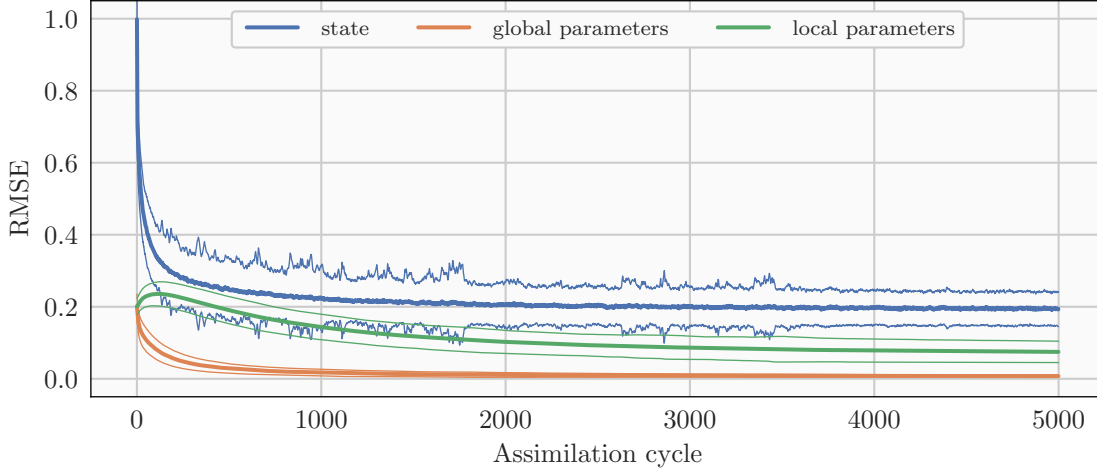


Figure 4: Time series of instantaneous analysis RMSE for the third test series (estimation of all 57 model coefficients) with the LEnSRF-HML. The state RMSE is shown in blue, the global parameter RMSE in yellow, and the local parameter RMSE in green. The experiment is repeated 1000 times, with different initial conditions and different observations. The thick line shows the average over all repetitions and the thin lines stand for the average plus or minus one standard deviation.

efficient. The minimal ensemble size  $N_e$  for a successful run has been reduced from 44 (without the LETKF-ML) to 20. Furthermore, the scores obtained by the LETKF-LML are qualitatively close to those obtained by the LETKF (with known model), although there is a small gap, which corresponds to the estimation of one additional parameter per grid point.

### 3.4.3 Estimation of all 57 model coefficients

In this third test series, the goal is to estimate the 17 monomial coefficients  $\mathbf{a}$  as well as the 40 forcing coefficients  $\mathbf{f}$ . The monomial coefficients  $\mathbf{a}$  must be included in the set of global parameters  $\mathbf{p}$ , while the forcing can be included in the set of local parameters  $\mathbf{q}$ . Hence, in these experiments there are  $N_p = 17$  global parameters and  $N_q = 40$  local parameters. The setup for each LEnKF-HML variant tested in this section is recalled in table 2 (last two rows).

The result of a first experiment with the LEnSRF-HML is shown in fig. 4. For this experiment, the ensemble size  $N_e$  is set to 36 and the specific values for the algorithmic parameters ( $r$ ,  $\lambda$ ,  $\zeta_p$ , and  $\zeta_q$ ) are chosen *by trial and error*. First of all, this experiment can be qualified as successful: after a spin-up period of several thousands of cycles, the state analysis RMSE stabilizes below 0.2. Second, the improvement of the analysis is overall rather slow. Parameter estimation in DA is slow in general, but it is here most likely due to a misspecification of the algorithmic parameters. For example, increasing the inflation factor  $\lambda$  could help at the beginning of the experiment, when the surrogate model is inaccurate, but would impair the analysis at the end of the experiment, when the surrogate model is more precise. Using adaptive parameters would resolve this dilemma, but this is beyond the scope of this paper<sup>4</sup>. Third, the algorithm improves the global parameter analysis before the local parameter analysis, the state analysis RMSE seems much more correlated to the global parameter analysis RMSE than to the local parameter analysis RMSE, and the final spread of the local parameter analysis RMSE is much larger than that of the global parameter analysis RMSE. All three elements are related to the fact that the surrogate model  $\text{sur}(\mathbf{a}, \mathbf{f})$  is more sensitive to a perturbation of the monomial coefficients  $\mathbf{a}$  (which are the global parameters  $\mathbf{p}$  in this experiment) than to a perturbation of the forcing coefficients  $\mathbf{f}$  (which are the local parameters  $\mathbf{q}$  in this experiment). Finally, the small increase in the local parameter analysis RMSE at the beginning of the experiment is once again most likely due to a misspecification of the algorithmic parameters.

After this first successful experiment, we wish to better characterize the function of each algorithmic parameters. While the role of the localization radius  $r$  and of the multiplicative inflation factor  $\lambda$  are well documented in the DA literature, this is not the case for the tapering coefficients  $\zeta_p$  and  $\zeta_q$ . For this reason, we show how the accuracy of the analysis depends on  $\zeta_p$  and  $\zeta_q$  in fig. 5. The state analysis RMSE is averaged over 10 000 cycles after a spin-up period of 10 000 cycles, and over 8 repetitions of the experiments. The ensemble size  $N_e$  is kept to 36 and in each case ( $\zeta_p$  and  $\zeta_q$ ), the values of the three other algorithmic parameters ( $r$ ,  $\lambda$ , and the other  $\zeta$ ) are optimally tuned to yield the lowest time-averaged state analysis RMSE.

<sup>4</sup>See (Bocquet *et al.*, 2020b) for an efficient example of adaptive inflation scheme but in the absence of localization.

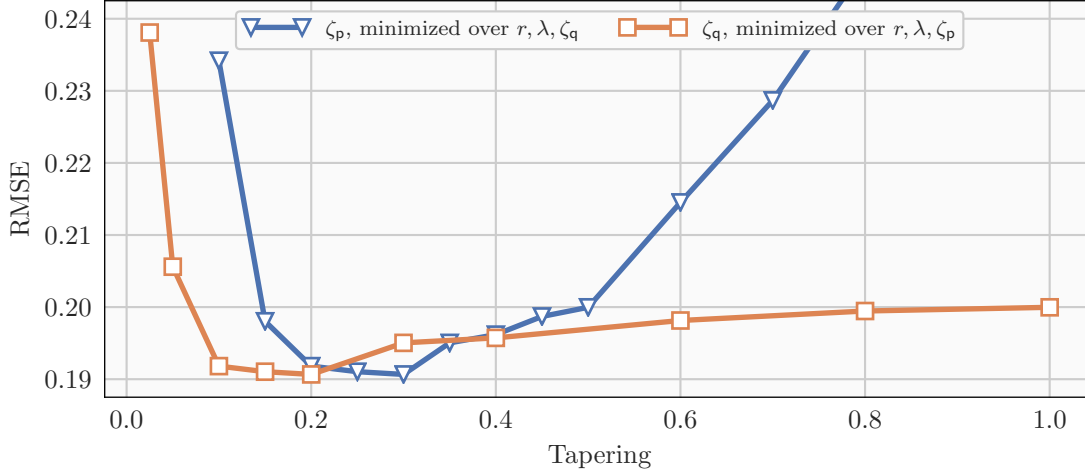


Figure 5: Time-averaged state analysis RMSE as a function of the global (in blue) and local (in yellow) tapering coefficient for the third test series (estimation of all 57 model coefficients) with the LEnSRF-HML.

Let us first discuss the global tapering coefficient  $\zeta_p$ . Without tapering ( $\zeta_p = 1$ ), the algorithm is unable to assimilate the observations. The global parameter update per cycle is too strong compared to the amount of information brought to the system by only one batch of observations. In a way, the algorithm is constantly overfitting the single batch of observations at each cycle. This issue is most likely due to the ensemble being too small to accurately represent the cross-correlations between state variables and global parameters, because, empirically, the need for tapering vanishes as the ensemble size grows (Bocquet *et al.*, 2020b). Hence,  $\zeta_p$  can here also be seen as a *relaxation* parameter. The analysis progressively improves as  $\zeta_p$  decreases, making the global parameter update slower but *more robust*. Finally, the state analysis RMSE reaches an optimal value and then grows again when the tapering is too strong. Indeed, for very small values of  $\zeta_p$ , the global parameter update is very slow, slow enough that the number of cycles used in the experiment, even though already large, is not enough to ensure the convergence of the statistics. Furthermore, as can be seen in fig. 5, lower values of the global tapering  $\zeta_p$ , typically below 0.1, yields numerical divergence of the filter since the relaxation to a better surrogate model is too slow.

The influence of the local tapering coefficient  $\zeta_q$  is qualitatively similar to that of  $\zeta_p$  with one exception. Even if using  $\zeta_q < 1$  yields better scores, tapering is not mandatory because the experiment is already successful without tapering ( $\zeta_q = 1$ ). This is most probably due to the fact that cross-correlations between state variables and local parameters are easier to estimate thanks to parameter localization.

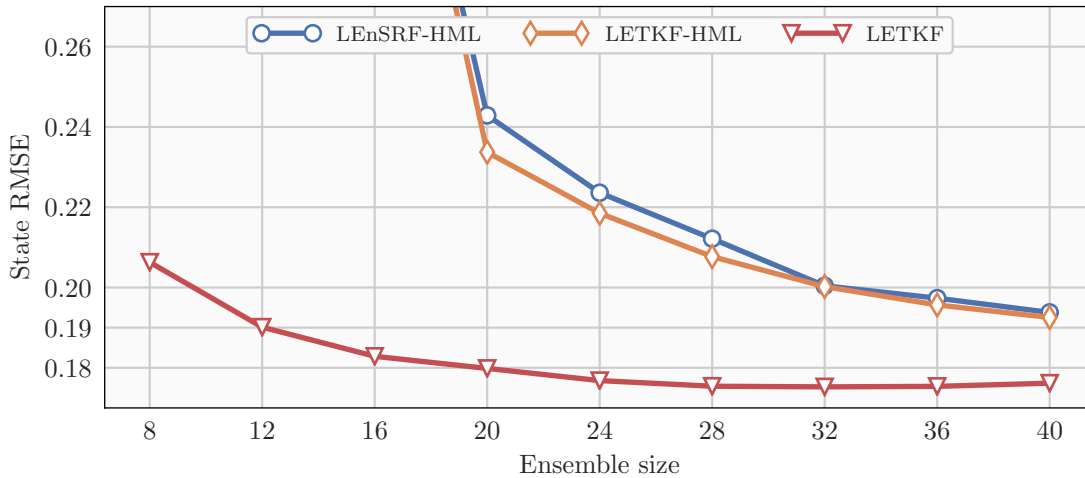


Figure 6: Time-averaged state analysis RMSE as a function of the ensemble size  $N_e$  for the third test series (estimation of all 57 model coefficients) with the LEnSRF-HML (in blue) and the LETKF-HML (in yellow). For reference, the green line shows the scores obtained with the LETKF when the model is known.

Finally, we show the accuracy of the analysis as a function of the ensemble size  $N_e$  in [fig. 6](#). The state analysis RMSE is averaged over 10 000 cycles after a spin-up period of 10 000 cycles, and over 8 repetition of the experiments.

First, there is almost no difference between the scores of the LEnSRF-HML and those of the LETKF-HML. The similarity between both algorithms can be explained using the same argument as for the similarity between the LEnSRF-ML and the LETKF-ML in [section 3.4.1](#). Second, two regimes can be qualitatively distinguished for the LEnKF-HML variants. When the ensemble size  $N_e$  is smaller than 20, the algorithms diverge, in a way which is very similar to the divergence of the LEnKF-ML variants in [section 3.4.1](#). When the ensemble size  $N_e$  is larger than 20, the accuracy of the analysis progressively improves, in a way which is very similar to the LETKF-LML in [section 3.4.2](#). These regimes can be explained as follows. In general, the LEnKF-HML estimates the most sensitive parameters first. In our experiments, the most sensitive parameters are the global parameters  $\mathbf{p}$ , which correspond to the 17 monomial coefficients  $\mathbf{a}$ . As for the LEnKF-ML, the minimal ensemble size  $N_e$  to estimate the state and the global parameters is around 20: 17 members for the  $N_p = 17$  global parameters (each global parameter is a neutral mode of the dynamics) plus a few additional members for the  $N_x = 40$  state variables (14 unstable and neutral modes, but the assimilation is localized). However, in this third test series, using  $N_e = 20$  is not sufficient because we must also estimate the  $N_q = 40$  local parameters. This explains the second regime which is qualitatively similar to the LETKF-LML. In this regime, we must add 12 additional members to decrease the analysis RMSE to 0.2. This is less than the additional  $N_q = 40$  local parameters to estimate, which shows that parameter localization is efficient. Eventually, for larger ensembles, the scores obtained by the LEnKF-HML variants become close to those obtained by the LETKF (with known model), with a small but meaningful gap corresponding to the additional estimation of the  $N_p = 17$  global parameters and of the  $N_q = 40$  local parameters.

## 4 Two dimensional illustration with global and local parameters, covariance and domain localizations

In this section, we provide an illustration of a selection of EnKF-HML algorithms with the multilayer L96 (mL96) model ([Farchi and Bocquet, 2019](#)), which is a two-dimensional extension of the standard L96 model with radiance-like (hence non-local) observations. This may seem a complicated example but it actually reflects to a large extent the requirements of a realistic, high-dimensional application of our methods.

### 4.1 The multilayer Lorenz 1996 model

The mL96 model consists in a vertical stack of  $N_v = 32$  coupled (atmospheric) layers, each layer being a one-dimensional L96 model with  $N_h = 40$  variables. The total state dimension is hence  $N_x = N_h \times N_v = 1280$ , and the model's equations are given by the following set of ODEs:

$$\frac{dx_{v,h}}{dt} = (x_{v,h+1} - x_{v,h-2})x_{v,h-1} - x_{v,h} + F_{v,h} + \Gamma_{v+1,h} - \Gamma_{v,h}, \quad (43)$$

where  $x_{v,h}$  is the  $h$ -th horizontal variable of the  $v$ -th vertical layer. The first terms in this equation correspond to the original L96 dynamics, where the horizontal index  $h$  applies periodically in  $\{1, \dots, N_h\}$ . The forcing term  $F$  is inhomogeneous; it is set constant over each layer and decreases from  $F_{1,h} = 8$  for the bottom layer to  $F_{N_v,h} = 4$  for the top layer. Finally, the last two terms correspond to the vertical coupling between adjacent layers, with

$$\Gamma_{v,h} \triangleq \begin{cases} x_{v,h} - x_{v-1,h} & \text{if } 2 \leq z \leq N_v, \\ 0 & \text{otherwise.} \end{cases} \quad (44)$$

The model is integrated using a fourth-order Runge–Kutta scheme with a time step of  $\delta t = 0.05$ . The dimension of the unstable and neutral subspace of the dynamics is about 50 ([Farchi and Bocquet, 2019](#)).

### 4.2 The surrogate model

For this two-dimensional illustration, we use the surrogate model presented in [section 3.2](#), which we adapt in the following way.

1. The 17 monomial coefficients  $\mathbf{a}$  are shared between all  $N_v$  layers.
2. In theory, the number of forcing coefficients of the model is  $N_v \times N_h$  (one for each state variable). To reduce this number and avoid an excessive initial underdetermination, we parameterize the forcing as  $F_{v,h} = F_v(v) \times F_h(h)$ , where  $F_v$  and  $F_h$  capture the vertical and horizontal variations of the forcing, respectively. The total number of forcing coefficients is hence  $N_v + N_h$ . However, to ensure the uniqueness of the decomposition,

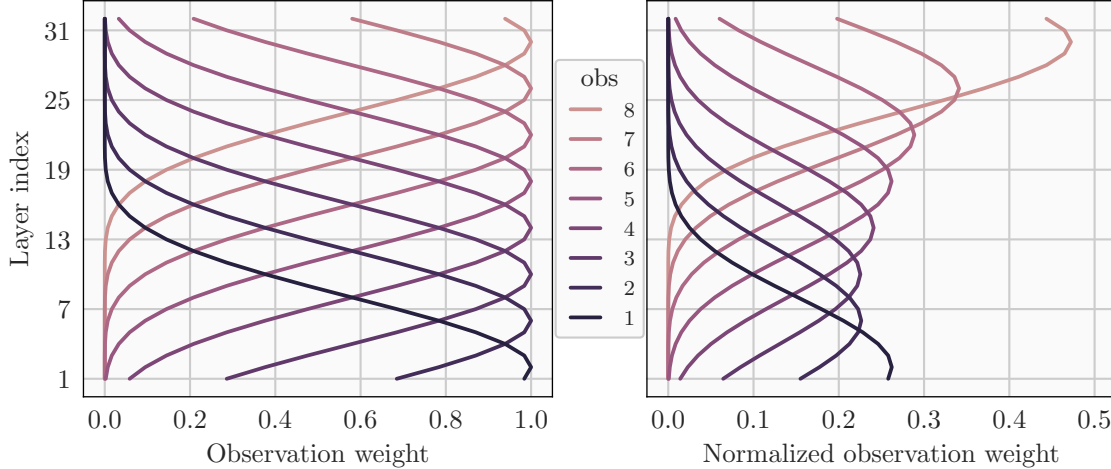


Figure 7: Averaging kernel for each of the 8 satellite channels with (right panel) and without (left panel) normalization.

we rescale  $F_v$  and  $F_h$  in such a way that  $F_v(0)$  is always 1. This reduces the effective number of forcing coefficients to  $N_v + N_h - 1$ .

3. The vertical coupling terms  $\Gamma_{v+1,h}$  and  $\Gamma_{v,h}$  are hard-coded in the model. In theory, these terms could have been learnt just as the rest of [eq. \(43\)](#), but it would make the illustration even more complex, which is why we chose not to.

As in [section 3.2](#), for convenience we introduce  $\text{sur}(\mathbf{a}, \mathbf{f}_v, \mathbf{f}_h)$  as the surrogate model in which the 17 monomial coefficients are  $\mathbf{a}$ , the  $N_v - 1 = 31$  vertical forcing coefficients are  $\mathbf{f}_v$  and the  $N_h = 40$  horizontal forcing coefficients are  $\mathbf{f}_h$ . The total number of parameters of this surrogate model is  $17 + 31 + 40 = 88$ . With this parameterization, the true mL96 model is identifiable: by construction it can be reproduced with a given set of parameters.

### 4.3 Experimental setup

#### 4.3.1 The inference problem

The experiments consist in twin simulations. The truth is generated using the mL96 model. At each time step  $\Delta t = 0.05$ , a total of  $N_y = 8 \times 40 = 320$  observations are generated, whose characteristics will be described in the next section.

In addition to estimating the state variables, the goal is to estimate the 17 monomial coefficients  $\mathbf{a}$ , the 40 horizontal forcings  $\mathbf{f}_h$  and the 31 vertical forcings in  $\mathbf{f}_v$ . In all experiments, the main performance metric is the time-averaged RMSE of the state analysis, as, in this context with very few parameters, a small state RMSE only can be obtained with successful parameter estimation.

#### 4.3.2 Observation setup

For this multilayer model, the observations consist in satellite soundings with 8 channels. Each channel is characterized by a vertical distribution of observation weights, also called averaging kernel, which is applied to all  $N_h = 40$  columns of state variables<sup>5</sup>.

The averaging kernels are constructed using the Gaspari–Cohn function, with centers evenly spaced along the vertical direction, and each with a half-width of 10 levels. They are independently normalized in such a way that the natural variability of each observation matches that of the L96i variables. The 8 non-normalized and normalized averaging kernels are displayed in [fig. 7](#). Finally, the observations are perturbed with a normal distribution of error covariance matrix  $\mathbf{R} = \mathbf{I}$ .

#### 4.3.3 The L2EnSRF-HML algorithm

With non-local observations such as the ones described above, using DL only yields suboptimal results. Therefore, following the approach of ([Farchi and Bocquet, 2019](#)), we include DL in the LEnSRF-HML, [algorithm 1](#), but only

<sup>5</sup>A column is defined here as the set of  $N_v = 32$  variables sharing the same horizontal index.

in the horizontal direction. The resulting  $L^2\text{EnSRF-HML}$  algorithm uses DL in the horizontal direction (in which observation are local) and CL in the vertical direction (in which observations are non-local). The analysis is summarized in [algorithm 3](#), in which several simplifications have been made.

- In principle, four categories of parameters exist: global, horizontally local, vertically local, and both horizontally and vertically local. [Algorithm 3](#) only uses two categories:  $\mathbf{q}$  gathers the set of horizontally local parameters and  $\mathbf{p}$  the set of horizontally non-local parameters. In both categories, the parameters can be vertically local or not.
- Vertical localization is performed using CL with the matrices  $\rho_{xx}$ ,  $\rho_{px}$  and  $\rho_{qx}$ .
- Horizontal localization is performed using DL with  $N_h$  local analyses. Each local analysis updates the  $h$ -th column of state variables and model parameters, whose indices are written  $c(h)$ , using a single localization matrix  $\rho_h$ , common to state variables and model parameters.

For our estimation problem, we split the surrogate model coefficients into  $\mathbf{p}$  and  $\mathbf{q}$  as follows. The 40 horizontal forcings coefficients  $\mathbf{f}_h$  are included in  $\mathbf{q}$ , and the 17 monomial coefficients  $\mathbf{a}$  are concatenated with the 31 vertical forcings coefficients  $\mathbf{f}_v$  to form the horizontally non-local parameters  $\mathbf{p}$ :

$$\mathbf{p} = \begin{bmatrix} \mathbf{a} \\ \mathbf{f}_v \end{bmatrix}. \quad (45)$$

---

### Algorithm 3 $L^2\text{EnSRF-HML}$ analysis

---

**Parameters:** Horizontal localization matrices  $\{\rho_h, h = 1, \dots, N_h\}$ , vertical localization matrices  $\rho_{xx}$ ,  $\rho_{px}$ , and  $\rho_{qx}$ , tapering parameters  $\zeta_p$  and  $\zeta_q$

**Input:** Forecast ensemble  $\mathbf{E}^f$

- 1:  $\bar{\mathbf{z}}^f = \mathbf{E}^f \mathbf{1} / N_e$
  - 2:  $\mathbf{X}^f = (\mathbf{E}^f - \bar{\mathbf{z}}^f \mathbf{1}^\top) / \sqrt{N_e - 1}$
  - 3:  $\mathbf{B}_{xx} = \rho_{xx} \circ [\mathbf{X}_x^f (\mathbf{X}_x^f)^\top]$
  - 4:  $\mathbf{B}_{qx} = \rho_{qx} \circ [\mathbf{X}_q^f (\mathbf{X}_x^f)^\top]$
  - 5:  $\mathbf{B}_{px} = \rho_{px} \circ [\mathbf{X}_p^f (\mathbf{X}_x^f)^\top]$
  - 6: **for**  $h = 1$  **to**  $N_h$  **do**
  - 7:  $\mathbf{R}_h^{-1} = \rho_h \circ \mathbf{R}^{-1}$
  - 8:  $\mathbf{T}_h = \mathbf{I} + \mathbf{R}_h^{-1/2} \mathbf{H}_x \mathbf{B}_{xx} \mathbf{H}_x^\top \mathbf{R}_h^{-1/2}$
  - 9:  $\mathbf{u}_x = \mathbf{H}_x^\top \mathbf{R}_h^{-1/2} \mathbf{T}_h^{-1} \mathbf{R}_h^{-1/2} (\mathbf{y} - \mathbf{H}_x (\bar{\mathbf{x}}^f))$
  - 10:  $\mathbf{U}_x = -\mathbf{H}_x^\top \mathbf{R}_h^{-1/2} (\mathbf{T}_h + \mathbf{T}_h^{1/2})^{-1} \mathbf{R}_h^{-1/2} \mathbf{H}_x (\mathbf{X}_x^f)$
  - 11:  $[\Delta \bar{\mathbf{x}}]_{c(h)} = [\mathbf{B}_{xx} \mathbf{u}_x]_{c(h)}$   $\triangleright$  state, mean update
  - 12:  $[\Delta \bar{\mathbf{q}}]_{c(h)} = \zeta_q [\mathbf{B}_{qx} \mathbf{u}_x]_{c(h)}$   $\triangleright$  horizontally local parameters, mean update
  - 13:  $[\Delta \mathbf{X}_x]_{c(h),:} = [\mathbf{B}_{xx} \mathbf{U}_x]_{c(h),:}$   $\triangleright$  state, perturbation update
  - 14:  $[\Delta \mathbf{X}_q]_{c(h),:} = \zeta_q [\mathbf{B}_{qx} \mathbf{U}_x]_{c(h),:}$   $\triangleright$  horizontally local parameters, perturbation update
  - 15:  $[\mathbf{V}_x]_{c(h),:} = [\mathbf{U}_x]_{c(h),:}$
  - 16:  $[\mathbf{v}_x]_{c(h)} = [\mathbf{u}_x]_{c(h)}$
  - 17: **end for**
  - 18:  $\Delta \bar{\mathbf{p}} = \zeta_p \mathbf{B}_{px} \mathbf{v}_x$   $\triangleright$  horizontally non-local parameters, mean update
  - 19:  $\Delta \mathbf{X}_p = \zeta_p \mathbf{B}_{px} \mathbf{V}_x$   $\triangleright$  horizontally non-local parameters, perturbation update
  - 20: **return**  $\mathbf{E}^a = (\bar{\mathbf{z}}^f + \Delta \bar{\mathbf{z}}) \mathbf{1}^\top + \sqrt{N_e - 1} (\mathbf{X}^f + \Delta \mathbf{X})$   $\triangleright$  Analysis ensemble
- 

#### 4.3.4 Ensemble initialization

The ensemble initialization is performed following the method described in [section 3.3.3](#). The state is initialized with a standard deviation of 0.5, smaller than in the one-dimensional test series because the time-averaged analysis error is expected to be smaller in the present experiment. The standard deviations for the horizontal and vertical forcing coefficients have been set to 0.17 and 0.012, respectively, in such a way that the initial RMSE for the 1280 reconstructed forcing coefficients (the outer product of the horizontal and vertical coefficients) is between 0.15 and 0.2. Finally, the

monomial coefficients initial standard deviation is set to  $\sigma_a = 0.1$ , once again smaller than in the one-dimensional test series as it makes the convergence faster.

### 4.3.5 Algorithm parameterization

As seen in [algorithm 3](#), the  $L^2$ EnSRF-HML analysis requires four kinds of localization matrices.

First, the horizontal localization matrices  $\rho_h$  are given by

$$[\rho_h]_{pq} \triangleq \sqrt{\text{GC} \left( \frac{2d_h(i, h)}{r_h} \right) \text{GC} \left( \frac{2d_h(j, h)}{r_h} \right)}, \quad (46)$$

where  $d_h(i, h)$  and  $d_h(j, h)$  are the horizontal (circular) distances between the  $i$ -th observation and the  $h$ -th column and between the  $j$ -th observation and the  $h$ -th column, respectively, and  $r_h$  is the horizontal localization radius.

Second, the vertical localization matrix between state variables,  $\rho_{xx}$ , is given by

$$[\rho_{xx}]_{mn} \triangleq \text{GC} \left( \frac{2d_v(m, n)}{r_v} \right), \quad (47)$$

where  $d_v(m, n)$  is the vertical distance between the  $m$ -th and  $n$ -th state variables and  $r_v$  is the vertical localization radius.

Third, the vertical cross-localization matrix between state variables and horizontally local parameters,  $\rho_{qx}$  is set to  $\mathbf{\Pi}$  because in this specific case the horizontally local parameters (the 40 horizontal forcing coefficients) are not vertically local.

Finally, the vertical cross-localization matrix between state variables and horizontally non-local parameters,  $\rho_{px}$  follows the same structure as the horizontally local parameters:

$$\rho_{px} = \begin{bmatrix} \mathbf{\Pi} \\ \rho_{vx} \end{bmatrix}, \quad (48)$$

where the first block, corresponding to the cross-localization between the monomial coefficients  $\mathbf{a}$  and the state variables, is set to  $\mathbf{\Pi}$ . Because the monomial coefficients are global, this matrix should be row-wise uniform, but we additionally assume it to be fully uniform for the sake of simplicity. The second block  $\rho_{vx}$ , corresponding to the cross-localization between the  $N_v - 1 = 31$  vertical forcing coefficients and the state variables, is given by

$$[\rho_{vx}]_{mn} \triangleq \text{GC} \left( \frac{2d_v(m, n)}{r_v} \right). \quad (49)$$

In this equation,  $d_v(m, n)$  is the vertical distance between the  $m$ -th vertical forcing coefficient and the  $n$ -th state variable, and  $r_v$  is the same vertical localization radius as in [eq. \(47\)](#) to reduce the number of algorithmic parameters. Note that, by construction, the  $m$ -th vertical forcing coefficient has the same vertical location as the  $(m + 1)$ -th state variable.

To summarize, the  $L^2$ EnSRF-HML analysis depends on two localization radii  $r_h$  and  $r_v$ . The analysis also depends on the two tapering coefficients  $\zeta_p$  and  $\zeta_q$ . In order to further reduce the number of algorithmic parameters, and given the results of [fig. 5](#), we set  $\zeta_p = \zeta_q \triangleq \zeta$ . Moreover, as in the one-dimensional test series, we use a multiplicative inflation on the prior with a uniform and constant in time coefficients  $\zeta$ . For each experiment, the algorithmic parameters  $(r_h, r_v, \zeta, \lambda)$  are tuned so as to yield optimal scores.

## 4.4 Results

The goal of the present test series is to show that it is possible to estimate the parameters of the surrogate model alongside the state variables, but also that parameter localization is efficient. To that purpose, we perform four types of experiments. We first test the  $L^2$ EnSRF-HML with and without localization. For comparison, we also test the  $L^2$ EnSRF, with known model, once again with and without localization. The results are described in the following sections, and summarized in [table 3](#).

### 4.4.1 Estimation of the state variables only

With known model, and without localization, 50 ensemble members are necessary to accurately estimate the 1280 state variables only, which corresponds more or less to the dimension of the unstable and neutral subspace ([Bocquet and Carrassi, 2017](#)). The time-averaged analysis RMSE is around 0.08. With localization, only 8 ensemble members ([Farchi et al., 2021b](#)) are required for a successful estimation, although the best scores require an ensemble of 10 members.

Table 3: Summary of the results for the two-dimensional test series with the mL96 model. For each experiment, we specify the inference problem (first column), the associated dimension of the unstable and neutral subspace of the augmented state dynamics  $N_0$  (second column), the analysis algorithm (third column), the forecast model (fourth column), whether localization is used or not (fifth column), the ensemble size  $N_e$  (seventh column), and the time-averaged state analysis RMSE (last column). The symbol  $\geq$  in the ensemble size column means that increasing the ensemble size does not yield significantly better scores.

Inference problem	$N_0$	Algorithm	Model	Loc.	$N_e$	state RMSE
1: $\mathbf{x}$	$\approx 50$	EnSRF	mL96		$\geq 50$	0.08
		L <sup>2</sup> EnSRF	mL96	✓	$\geq 10$	0.08
2: $(\mathbf{x}, \mathbf{a}, \mathbf{f}_v, \mathbf{f}_h)$	$\approx 50 + 88$	EnSRF-HML	sur $(\mathbf{a}, \mathbf{f}_v, \mathbf{f}_h)$		$\geq 140$	0.11
		L <sup>2</sup> EnSRF-HML	sur $(\mathbf{a}, \mathbf{f}_v, \mathbf{f}_h)$	✓	50	0.12

#### 4.4.2 Estimation of both state variables and model parameters without localization

Without localization, an ensemble of 140 members is sufficient to accurately estimate the 88 model parameters alongside the 1280 state variables. The time-averaged state analysis is around 0.11. Although this experiment is not the main result of the present two-dimensional test series, we think that it provides a reasonable approximation of the best scores that can be obtained with the L<sup>2</sup>EnSRF-HML.

More precisely, we have found that the state analysis RMSE decreases almost linearly as the ensemble size  $N_e$  increases (not shown here). The score stops improving when  $N_e$  reaches a critical value, around  $N_e = 140$  here, which is close to the dimension of the unstable and neutral subspace of the augmented state dynamics (Bocquet *et al.*, 2020b). When the ensemble size  $N_e$  is close, but smaller to 140, the algorithm is able to accurately estimate the monomial coefficients  $\mathbf{a}$  but struggles to estimate the forcing coefficients  $\mathbf{f}_v$  and  $\mathbf{f}_h$ . This is once again related to the fact that the surrogate model is more sensitive to a perturbation of  $\mathbf{a}$ .

#### 4.4.3 Estimation of both state variables and model parameters with localization

With localization, an ensemble of only 50 members is sufficient to accurately estimate the 88 model parameters alongside the state. From the previous experiments, we know that 10 members are sufficient to estimate the state variables. Additionally, 17 members are required to estimate the 17 monomial coefficients  $\mathbf{a}$ , which are neutral modes of the augmented state dynamics and which do not benefit from localization. This means that only  $50 - 10 - 17 = 23$  members are necessary to estimate the  $40 + 31 = 71$  horizontal and vertical forcing coefficients  $\mathbf{f}_v$  and  $\mathbf{f}_h$ . This shows that parameter localization is indeed effective.

For this inference problem, fig. 8 shows the results of an experiment with 50 members. The conclusions are overall very similar to those in section 3.4.3. First, the experiment can be qualified as successful: after a spin-up period of several hundreds of cycles, the state analysis RMSE stabilizes around 0.12. Second, the improvement of the analysis is rather slow, once again because the algorithmic parameters have been chosen to minimize the analysis error at the end of the experiment. Third, the different components of the augmented state are learnt on different time scales: the algorithm first corrects the state and the monomial coefficients  $\mathbf{a}$ , which are the most sensitive parameters. Finally, note that the time-averaged state analysis RMSE is a bit higher here (0.12) than in section 4.4.2 without localization (0.11), but we have checked that better scores can be obtained with localization when using larger ensembles.

## 5 Conclusions

Piggybacking on the results of (Bocquet *et al.*, 2020b), we have shown how the classical LETKF and LEnSRF can be generalized to estimate model parameters, both global and local, alongside the state variables. The assimilation of local parameters is natural with DL (*i.e.* the LETKF), especially when model parameters and state variables are co-located. By contrast, CL (*i.e.* the LEnSRF) is more suited than DL to the estimation of global parameters, and to the assimilation of non-local observations, at the cost of having to perform linear algebra in the whole state space. Introducing the ancillary variables defined in eq. (17a) and eq. (17b) for the LEnSRF-HML, and defined in eq. (35a) and eq. (35b) for the LETKF-HML, we have optimized these algorithms in such a way that it is not necessary to compute  $\mathbf{B}_{xx}^{-1}$  when evaluating the global parameter update from the local state update. Moreover, we have shown how to rigorously assimilate global parameters within the DL-based LETKF, assuming the observations are local. The existing and proposed algorithms are summarized in table 4.

Introducing the L96i, an inhomogeneous variant of the L96 model, we have numerically tested the LETKF-HML and the LEnSRF-HML. The results are overall consistent with those of (Bocquet *et al.*, 2020b), they show that the

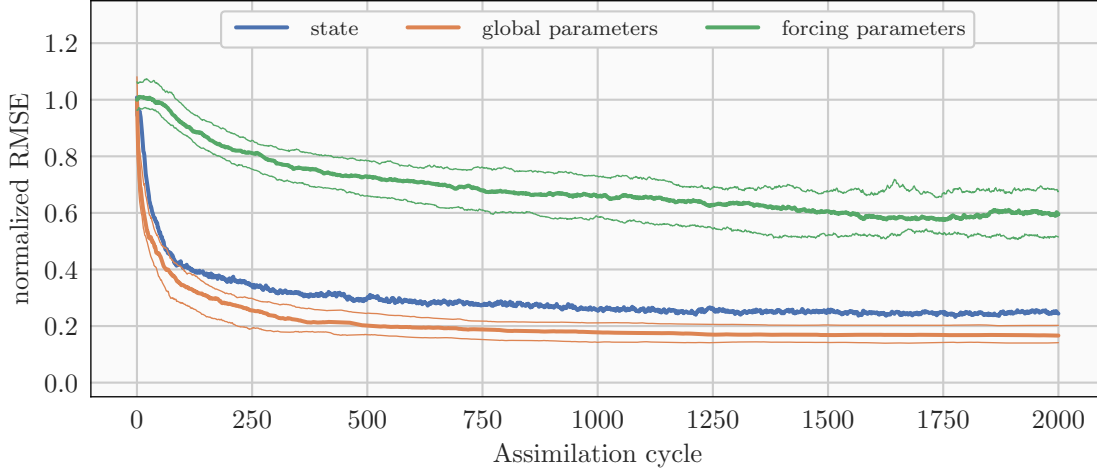


Figure 8: Time series of instantaneous analysis RMSE for the two-dimensional test series (with the mL96 model) using the  $L^2\text{EnSRF-HML}$ . The state RMSE is shown in blue, the RMSE for the 17 monomial coefficients  $\mathbf{a}$  in yellow, and the RMSE for the 1280 reconstructed forcing coefficients (the outer product of the horizontal and vertical coefficients) in green. In all cases, the RMSE is normalized by its initial value. The thick lines represent the median over 100 experiments, and the thin lines represent the 32-th and 68-th percentiles. For clarity purposes, the dispersion of the state RMSE is not represented, since it is very small.

algorithms are able to learn the dynamics of a fully parameterized surrogate model alongside the state variables, and that parameter localization is beneficial, in the sense that it is possible to estimate a large amount of parameters with reasonable ensemble sizes.

Finally, we have generalized the  $L^2\text{EnSRF}$  algorithm proposed in (Farchi *et al.*, 2021b) to estimate model parameters alongside the state variables. The resulting algorithm, called  $L^2\text{EnSRF-HML}$ , combines DL in the horizontal direction and CL in the vertical direction, and is able to take into account the local nature of state variables and model parameters in both the horizontal and vertical directions. We have illustrated with success the algorithm using a multilayer L96 experiment with radiance-like, non-local observations, in which the surrogate model has global monomial coefficients as well as vertically local and horizontally local forcing coefficients.

Multiple investigations could be initiated following this paper. First, we have shown that using non-adaptive algorithmic parameters can be critical because the optimal algorithmic parameters change over time, as the surrogate model progressively improves. Second, we restricted our numerical studies to fully observed systems. Showing results for systems with sparse observations is interesting *per se*, but we suspect that it could be a way to clearly distinguish the LETKF-Aksoy from the LETKF-ML. Third, the online characteristics of the proposed algorithms could be exploited in situations with slow parameter time evolution, while offline algorithms would be unfit to this task. Finally, a next goal would be to learn the dynamics of more complex and non identifiable surrogate representations, with a more realistic dynamical model (both in term of physical interpretation and of state dimension).

## A Proof of the corrected ETKF-ML formulae

In this appendix, we provide a proof of eq. (35), which is the core of the ETKF-ML parameter update. Let us start with  $\mathbf{u}_x$ . From eqs. (13) and (17a), we have

$$\mathbf{u}_x = \mathbf{H}_x^\top \left( \mathbf{R} + \mathbf{H}\mathbf{B}\mathbf{H}^\top \right)^{-1} \mathbf{d}, \quad (50)$$

where  $\mathbf{d}$  is the innovation vector defined as

$$\mathbf{d} \triangleq \mathbf{y} - \mathbf{H}(\bar{\mathbf{z}}^f). \quad (51)$$

Using the ETKF ancillary variables eq. (30), we conclude

$$\mathbf{u}_x = \mathbf{H}_x^\top \mathbf{R}^{-1} \left( \mathbf{I} + \mathbf{Y}\mathbf{Y}^\top \mathbf{R}^{-1} \right)^{-1} \mathbf{d}, \quad (52)$$

$$= \mathbf{H}_x^\top \mathbf{R}^{-1} \left( \mathbf{I} + \mathbf{Y}\mathbf{Y}^\top \mathbf{R}^{-1} \right)^{-1} \left( \mathbf{I} + \mathbf{Y}\mathbf{Y}^\top \mathbf{R}^{-1} - \mathbf{Y}\mathbf{Y}^\top \mathbf{R}^{-1} \right) \mathbf{d}, \quad (53)$$

$$= \mathbf{H}_x^\top \mathbf{R}^{-1} \left\{ \mathbf{I} - \left( \mathbf{I} + \mathbf{Y}\mathbf{Y}^\top \mathbf{R}^{-1} \right)^{-1} \mathbf{Y}\mathbf{Y}^\top \mathbf{R}^{-1} \right\} \mathbf{d}, \quad (54)$$

$$= \mathbf{H}_x^\top \mathbf{R}^{-1} \left\{ \mathbf{d} - \mathbf{Y} \left( \mathbf{I} + \mathbf{Y}^\top \mathbf{R}^{-1} \mathbf{Y} \right)^{-1} \mathbf{Y}^\top \mathbf{R}^{-1} \mathbf{d} \right\}, \quad (55)$$

$$= \mathbf{H}_x^\top \mathbf{R}^{-1} (\mathbf{d} - \mathbf{Y}\mathbf{w}^a), \quad (56)$$

which is eq. (35a). Note that eq. (55) is obtained from eq. (54) using the matrix shift lemma.

Likewise, from eqs. (13) and (17b), we have

$$\mathbf{U}_x = \mathbf{H}_x^\top \left\{ \mathbf{R} + \mathbf{H}\mathbf{B}\mathbf{H}^\top + \mathbf{R} \left( \mathbf{I} + \mathbf{R}^{-1} \mathbf{H}\mathbf{B}\mathbf{H}^\top \right)^{1/2} \right\}^{-1} \mathbf{H} (\mathbf{X}^f), \quad (57)$$

$$= \mathbf{H}_x^\top \left\{ \mathbf{I} + \mathbf{R}^{-1} \mathbf{H}\mathbf{B}\mathbf{H}^\top + \left( \mathbf{I} + \mathbf{R}^{-1} \mathbf{H}\mathbf{B}\mathbf{H}^\top \right)^{1/2} \right\}^{-1} \mathbf{R}^{-1} \mathbf{H} (\mathbf{X}^f), \quad (58)$$

$$= \mathbf{H}_x^\top \left\{ \mathbf{I} + \mathbf{R}^{-1} \mathbf{Y}\mathbf{Y}^\top + \left( \mathbf{I} + \mathbf{R}^{-1} \mathbf{Y}\mathbf{Y}^\top \right)^{1/2} \right\}^{-1} \mathbf{R}^{-1} \mathbf{Y}, \quad (59)$$

$$= \mathbf{H}_x^\top \mathbf{R}^{-1} \mathbf{Y} \left\{ \mathbf{I} + \mathbf{Y}^\top \mathbf{R}^{-1} \mathbf{Y} + \left( \mathbf{I} + \mathbf{Y}^\top \mathbf{R}^{-1} \mathbf{Y} \right)^{1/2} \right\}^{-1}, \quad (60)$$

$$= \mathbf{H}_x^\top \mathbf{R}^{-1} \mathbf{Y} \left( \mathbf{T} + \mathbf{T}^{1/2} \right)^{-1}, \quad (61)$$

which is eq. (35b). Note that eq. (60) is obtained from eq. (59) using once again the matrix shift lemma.

## B General state variables and global parameter covariance matrix

In this appendix, we focus on the global parameter problem and consider the most general cross localization matrix given by eq. (22). We would like to improve on Section 3.2.4 of (Bocquet *et al.*, 2020b) where the global parameters have been considered statistically homogeneous, such that  $\zeta_p = \zeta_p \mathbf{1}_p$  was posed. The most general form of the localization matrix is then:

$$\boldsymbol{\rho} = \begin{bmatrix} \boldsymbol{\rho}_{xx} & \mathbf{\Pi}_{xp} \text{diag}(\zeta_p) \\ \text{diag}(\zeta_p) \mathbf{\Pi}_{px} & \boldsymbol{\rho}_{pp} \end{bmatrix}. \quad (62)$$

For  $\boldsymbol{\rho}$  to be a correlation matrix, this implies constraints on the vector of tapering coefficients  $\zeta_p$ . Assuming  $\boldsymbol{\rho}_{xx}$  is positive definite,  $\boldsymbol{\rho}$  is positive semi-definite if and only if the Schur complement

$$\mathbf{S}_{pp} = \boldsymbol{\rho}_{pp} - \text{diag}(\zeta_p) \mathbf{\Pi}_{px} \boldsymbol{\rho}_{xx}^{-1} \mathbf{\Pi}_{xp} \text{diag}(\zeta_p) \quad (63)$$

is positive semi-definite.

Alternatively, assuming  $\boldsymbol{\rho}_{pp}$  is positive definite,  $\boldsymbol{\rho}$  is positive semi-definite if and only if the Schur complement

$$\mathbf{S}_{xx} = \boldsymbol{\rho}_{xx} - \mathbf{\Pi}_{xp} \text{diag}(\zeta_p) \boldsymbol{\rho}_{pp}^{-1} \text{diag}(\zeta_p) \mathbf{\Pi}_{px} \quad (64)$$

is positive semi-definite.

Both conditions can be re-arranged as

$$\mathbf{S}_{pp} = \boldsymbol{\rho}_{pp} - \mathbf{1}_x^\top \boldsymbol{\rho}_{xx}^{-1} \mathbf{1}_x \cdot \zeta_p \zeta_p^\top, \quad (65)$$

and

$$\mathbf{S}_{xx} = \boldsymbol{\rho}_{xx} - \zeta_p^\top \boldsymbol{\rho}_{pp}^{-1} \zeta_p \cdot \mathbf{\Pi}_{xx}. \quad (66)$$

Since the second term on the right-hand-side of eq. (65) is of rank one, we only need to ensure that the condition is true along  $\zeta_{pp}$ :

$$\zeta_p^\top \mathbf{S}_{pp} \zeta_p = \zeta_p^\top \boldsymbol{\rho}_{pp} \zeta_p - \mathbf{1}_x^\top \boldsymbol{\rho}_{xx}^{-1} \mathbf{1}_x \cdot \|\zeta_p\|^4 \geq 0, \quad (67)$$

Table 4: Summary of the EnKF-ML family of algorithms

Inference problem	Dom. Local. local obs. only	Cov. Local. numerically costly	Dom. + Cov. Local.
State	LETKF (Hunt <i>et al.</i> , 2007)	LEnSRF (Whitaker and Hamill, 2002)	L <sup>2</sup> EnSRF (Farchi and Bocquet, 2019)
State + global param.	LETKF-ML (Bocquet <i>et al.</i> , 2020b) new implementation	LEnSRF-ML (Bocquet <i>et al.</i> , 2020b) new implementation	L <sup>2</sup> EnSRF-ML not discussed
State + global & local param.	LETKF-HML new algorithm	LEnSRF-HML new algorithm	L <sup>2</sup> EnSRF-HML new algorithm

where  $\|\cdot\|$  is the Euclidean norm.

Likewise, since the second term on the right-hand-side of eq. (66) is of rank one, we only need to ensure that the condition is true along  $\mathbf{1}_x$ :

$$\mathbf{1}_x^\top \mathbf{S}_{xx} \mathbf{1}_x = \mathbf{1}_x^\top \boldsymbol{\rho}_{xx} \mathbf{1}_x - \boldsymbol{\zeta}_p^\top \boldsymbol{\rho}_{pp}^{-1} \boldsymbol{\zeta}_p N_x^2 \geq 0. \quad (68)$$

As a consequence, a sufficient condition for the positivity of  $\boldsymbol{\rho}$  that can be easily derived from *both* of these scalar conditions, is

$$\|\boldsymbol{\zeta}_p\| \leq \sqrt{\frac{\lambda_p^{\min} \lambda_x^{\min}}{N_x}}, \quad (69)$$

where  $\lambda_p^{\min}$ ,  $\lambda_x^{\min}$  are the smallest eigenvalues of  $\boldsymbol{\rho}_{pp}$ ,  $\boldsymbol{\rho}_{xx}$ , respectively. This result includes the more heuristic and less general equation (26) of (Bocquet *et al.*, 2020b). This upper bound is very likely to be suboptimal but it suggests that it scales in the state space dimension as  $N_x^{-1/2}$ .

## C Summary of the presented algorithms

The local EnKF-based methods for estimating state, global and both local and global parameters are summarized in table 4.

## Acknowledgments

CEREA is a member of Institut Pierre-Simon Laplace (IPSL).

## References

- Asky, A., Zhang, F. and Nielsen-Gammon, J. (2006). Ensemble-based simultaneous state and parameter estimation in a two-dimensional sea-breeze model. *Mon. Wea. Rev.*, 134, 2951–2969. doi:10.1175/MWR3224.1.
- Arcomano, T., Szunyogh, I., Pathak, J., Wikner, A., Hunt, B. R. and Ott, E. (2020). A machine learning-based global atmospheric forecast model. *Geophys. Res. Lett.*, 47, e2020GL087776. doi:10.1029/2020GL087776.
- Arcucci, R., Zhu, J., Hu, S. and Guo, Y.-K. (2021). Deep data assimilation: Integrating deep learning with data assimilation. *Applied Sciences*, 11, 1114. doi:10.3390/app11031114.
- Asch, M., Bocquet, M. and Nodet, M. (2016). *Data Assimilation: Methods, Algorithms, and Applications*. Fundamentals of Algorithms. : SIAM, Philadelphia.
- Bocquet, M., Brajard, J., Carrassi, A. and Bertino, L. (2019). Data assimilation as a learning tool to infer ordinary differential equation representations of dynamical models. *Nonlin. Processes Geophys.*, 26, 143–162. doi:10.5194/npg-26-143-2019.
- Bocquet, M., Brajard, J., Carrassi, A. and Bertino, L. (2020). Bayesian inference of chaotic dynamics by merging data assimilation, machine learning and expectation-maximization. *Foundations of Data Science*, 2, 55–80. doi:10.3934/fods.2020004.
- Bocquet, M. and Carrassi, A. (2017). Four-dimensional ensemble variational data assimilation and the unstable subspace. *Tellus A*, 69, 1304504. doi:10.1080/16000870.2017.1304504.
- Bocquet, M. and Farchi, A. (2019). On the consistency of the local ensemble square root kalman filter perturbation update. *Tellus A: Dynamic Meteorology and Oceanography*, 71 (1), 1–21. doi:10.1080/16000870.2019.1613142.

- Bocquet, M., Farchi, A. and Malartic, Q. (2020). Online learning of both state and dynamics using ensemble Kalman filters. *Foundations of Data Science*, 0, 00–00. doi:10.3934/fods.2020015, accepted for publication.
- Bocquet, M. and Sakov, P. (2013). Joint state and parameter estimation with an iterative ensemble Kalman smoother. *Nonlin. Processes Geophys.*, 20, 803–818. doi:10.5194/npg-20-803-2013.
- Boyd, S., Parikh, N., Chu, E., Peleato, B. and Eckstein, J. (2011). Distributed optimization and statistical learning via the alternating direction method of multipliers. *Found. Trends Mach. Learn.*, 3, 1–122. doi:10.1561/22000000016.
- Brajard, J., Carrassi, A., Bocquet, M. and Bertino, L. (2020). Combining data assimilation and machine learning to emulate a dynamical model from sparse and noisy observations: a case study with the Lorenz 96 model. *J. Comput. Sci.*, 44, 101171. doi:10.1016/j.jocs.2020.101171.
- Brajard, J., Carrassi, A., Bocquet, M. and Bertino, L. (2021). Combining data assimilation and machine learning to infer unresolved scale parametrisation. *Phil. Trans. R. Soc. A*, 379, 20200086. doi:10.1098/rsta.2020.0086.
- Brunton, S. L., Proctor, J. L. and Kutz, J. N. (2016). Discovering governing equations from data by sparse identification of nonlinear dynamical systems. *PNAS*, 113, 3932–3937. doi:10.1073/pnas.1517384113.
- Dueben, P. D. and Bauer, P. (2018). Challenges and design choices for global weather and climate models based on machine learning. *Geosci. Model Dev.*, 11, 3999–4009. doi:10.5194/gmd-11-3999-2018.
- Evensen, G. (2009). *Data Assimilation: The Ensemble Kalman Filter*, 2nd Edition. : Springer-Verlag Berlin Heidelberg.
- Fablet, R., Ouala, S. and Herzet, C. (2018). Bilinear residual neural network for the identification and forecasting of dynamical systems. In: *EUSIPCO 2018, European Signal Processing Conference*. Rome, Italy, pp. 1–5.
- Farchi, A. and Bocquet, M. (2019). On the efficiency of covariance localisation of the ensemble Kalman filter using augmented ensembles. *Front. Appl. Math. Stat.*, 5, 3. doi:10.3389/fams.2019.00003.
- Farchi, A., Bocquet, M., Laloyaux, P., Bonavita, M. and Malartic, Q. (2021). A comparison of combined data assimilation and machine learning methods for offline and online model error correction, 0, 0. Submitted.
- Farchi, A., Laloyaux, P., Bonavita, M. and Bocquet, M. (2021). Using machine learning to correct model error in data assimilation and forecast applications. *Q. J. R. Meteorol. Soc.*, 0, 0. Accepted for publication.
- Fertig, E., Baek, S.-J., Hunt, B., Ott, E., Szunyogh, I., Aravéquia, J., Kalnay, E., Li, H. and Liu, J. (2009). Observation bias correction with an ensemble Kalman filter. *Tellus A*, 61, 210–226. doi:10.1111/j.1600-0870.2008.00378.x.
- Gaspari, G. and Cohn, S. E. (1999). Construction of correlation functions in two and three dimensions. *Quarterly Journal of the Royal Meteorological Society*, 125 (554), 723–757. doi:10.1002/qj.49712555417.
- Harlim, J. (2018). *Data-driven computational methods: parameter and operator estimations*. : Cambridge University Press, Cambridge.
- Hu, X.-M., Zhang, F. and Nielsen-Gammon, J. W. (2010). Ensemble-based simultaneous state and parameter estimation for treatment of mesoscale model error: A real-data study. *Geophys. Res. Lett.*, 37, L08802. doi:10.1029/2010GL043017.
- Hunt, B. R., Kostelich, E. J. and Szunyogh, I. (2007). Efficient data assimilation for spatiotemporal chaos: A local ensemble transform Kalman filter. *Physica D*, 230, 112–126. doi:10.1016/j.physd.2006.11.008.
- Jazwinski, A. H. (1970). *Stochastic Processes and Filtering Theory*. : Academic Press, New-York.
- Koyama, H. and Watanabe, M. (2010). Reducing forecast errors due to model imperfections using ensemble Kalman filtering. *Mon. Wea. Rev.*, 138, 3316–3332. doi:10.1175/2010MWR3067.1.
- Lguensat, R., Tandeo, P., Ailliot, P., Pulido, M. and Fablet, R. (2017). The analog data assimilation. *Mon. Wea. Rev.*, 145, 4093–4107. doi:10.1175/MWR-D-16-0441.1.
- Lorenz, E. N. and Emanuel, K. A. (1998). Optimal sites for supplementary weather observations: Simulation with a small model. *Journal of the Atmospheric Sciences*, 55 (3), 399–414. doi:10.1175/1520-0469(1998)055<0399:OSFSWO>2.0.CO;2.
- Nerger, L. and Gregg, W. W. (2007). Assimilation of SeaWiFS data into a global ocean-biogeochemical model using a local SEIK filter. *Journal of Marine Systems*, 68, 237–254. doi:10.1016/j.jmarsys.2006.11.009.
- Pathak, J., Hunt, B., Girvan, M., Lu, Z. and Ott, E. (2018). Model-free prediction of large spatiotemporally chaotic systems from data: A reservoir computing approach. *Phys. Rev. Lett.*, 120, 024102. doi:10.1103/PhysRevLett.120.024102.
- Ruckstuhl, Y. M. and Janjić, T. (2018). Parameter and state estimation with ensemble Kalman filter based algorithms for convective-scale applications. *Q. J. R. Meteorol. Soc.*, 144, 826–841. doi:10.1002/qj.3257.

- Ruiz, J. J., Pulido, M. and Miyoshi, T. (2013). Estimating model parameters with ensemble-based data assimilation: A review. *J. Meteorol. Soc. Japan*, 91, 79–99. doi:10.2151/jmsj.2013-201.
- Sakov, P. and Bertino, L. (2011). Relation between two common localisation methods for the EnKF. *Comput. Geosci.*, 15, 225–237. doi:10.1007/s10596-010-9202-6.
- Scher, S. and Messori, G. (2019). Generalization properties of feed-forward neural networks trained on Lorenz systems. *Nonlin. Processes Geophys.*, 26, 381–399. doi:10.5194/npg-26-381-2019.
- Weyn, J. A., Durran, D. R. and Caruana, R. (2019). Using deep learning to predict gridded 500-hPa geopotential height from historical weather data. *Journal of Advances in Modeling Earth Systems*, 11, 2680–2693. doi:10.1029/2019MS001705.
- Whitaker, J. S. and Hamill, T. M. (2002). Ensemble data assimilation without perturbed observations. *Mon. Wea. Rev.*, 130 (7), 1913–1924. doi:10.1175/1520-0493(2002)130<1913:EDAWPO>2.0.CO;2.
- Wikner, A., Pathak, J., Hunt, B., Girvan, M., Arcomano, T., Szunyogh, I., Pomerance, A. and Ott, E. (2020). Combining machine learning with knowledge-based modeling for scalable forecasting and subgrid-scale closure of large, complex, spatiotemporal systems. *Chaos: An Interdisciplinary Journal of Nonlinear Science*, 30, 053111. doi:10.1063/5.0005541.